Kinetic study of azobenzene E/Z isomerization using ion mobility-mass spectrometry and liquid chromatography-UV detection

Salomé Poyer, Chang Min Choi, Claire Deo, Nicolas Bogliotti, Juan Xie, Philippe Dugourd, Fabien Chirot, Jean-Yves Salpin

Kinetic study of azobenzene *E*/*Z* isomerization using ion mobility-mass spectrometry and liquid chromatography-UV detection.

Salomé Poyer[1,2*], Chang Min Choi[3], Claire Deo[4], Nicolas Bogliotti[4], Juan Xie[4], Philippe Dugourd[5], Fabien Chirot[6], Jean-Yves Salpin.[1,2*]

[1] Université Paris-Saclay, Univ Evry, CNRS, LAMBE, 91025, Evry-Courcouronnes, France

[2] CY Cergy Paris Université, CNRS, LAMBE, 95000, Cergy, France

[3] Center for Scientific Instrumentation, Korea Basic Science Institute, Chungbuk, Republic of Korea

[4.] Université Paris-Saclay, ENS Paris-Saclay, CNRS, PPSM, 94235 Cachan, France

[5.] Univ Lyon, Université Claude Bernard Lyon 1, CNRS, UMR5306 Institut Lumière Matière, 69622 Villeurbanne, France

[6.] Univ Lyon, Université Claude Bernard Lyon 1, CNRS, ENS de Lyon, UMR5280 Institut des Sciences Analytiques, F-69622 Villeurbanne, France

Direct link to the editor (RSC): https://doi.org/10.1039/D0AN00048E

ABSTRACT:

Z and *E* azobenzene isomers are molecular switches which can interconvert both photochemically and thermally. Presently, we studied a ketal-substituted bridged azobenzene in which two stable diastereomeric conformers (*Z1* and *Z2*) photochemically interconvert through transient *E* isomer. UV-VIS absorption spectroscopy is commonly used to study the relaxation kinetics of azobenzenes, but it does not allow direct quantitation of the process in this case. In the present paper, liquid chromatography coupled to UV detection (LC-UV) and ion mobility-mass spectrometry (IMS-MS) were combined to study the thermal back relaxation kinetics of the *E* isomer. LC separation of the three isomers was achieved in less than 10 minutes, allowing the characterization of the relatively slow thermal back relaxation kinetics at low temperature through UV detection. In addition, the faster *E*→*Z* thermal back relaxation at higher temperature was studied using IMS-MS, which allows shorter time scale separation than LC. Baseline separation of the two *Z* isomers was achieved in IMS-MS for $[Z+Ag]^+$ ions, and their gas-phase conformations were determined by IRMPD experiments. Both IMS-MS and LC-UV methodologies succeeded to study the *E*→*Z* thermal back relaxation kinetics, and appeared to be complementary techniques. We show that the combination of the two techniques allows the characterization of the isomerization processes over a broad temperature range, and the determination of the associated thermodynamic observables.

INTRODUCTION

Photochromic molecules undergo reversible transformation between two forms (exhibiting different absorption spectra) upon exposure to light of appropriate wavelength.[1] This process results in important changes, both at the structural and electronic levels. Due to this peculiarity, photoisomerization of photochromic compounds is currently being applied to the control of biological activity,[2-4] chemical reactivity,[5-7] or supramolecular assemblies.[8-11] Azobenzene derivatives are among the most widely used photoswitchable molecules due to their usually straightforward synthesis and functionalization, allowing the tuning of their optical and physico-chemical properties.[12-15] For this class of compounds, reversible $E \leftrightarrow Z$ photoisomerization generally occurs upon irradiation with UV or visible light, leading to significant changes in properties between the thermodynamically favored planar *E* isomer and the metastable non-planar *Z* isomer.

However, these photochromic properties are strongly influenced by the environment (temperature, solvent, irradiation time, etc.). This can make challenging the quantification of the relative proportion of (*Z*) and (*E*) isomers based on classical characterization techniques (UV-VIS or NMR), especially when species are in low concentrations or within complex mixtures. This is especially the case for bridged azobenzenes, characterized by a *Z*-isomer more stable than the highly twisted *E*-isomer, due to the ring strain.[16]

The synthesis and isomerization properties of ketal-substituted bridged azobenzenes, presenting a highly twisted unstable *E* isomer has recently been reported.[17] A particularity of this system is the existence of two stable *Z* diastereoisomers namely *Z1* and *Z2* (Scheme 1), whose relative proportions can be varied depending on the irradiation wavelength.[17] This uncommon three-component switching system proved especially challenging to analyze by UV-VIS absorption spectroscopy, because no characteristic wavelength allows the quantitation for $E \rightarrow Z$ thermal back relaxation process.

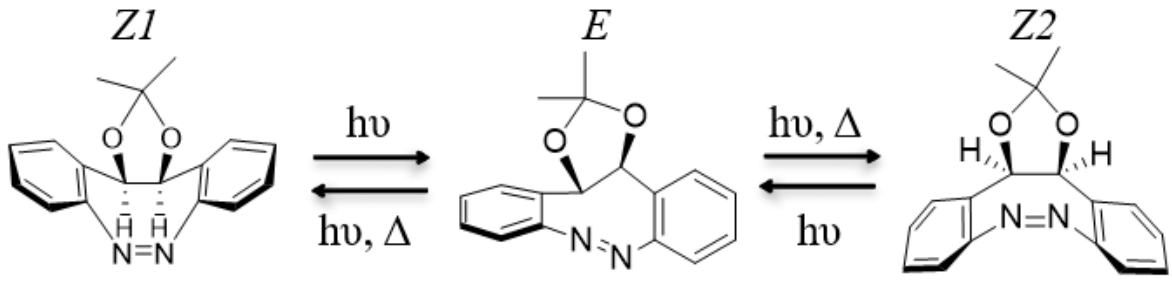

Scheme 1. Thermal- and photo-induced isomerization pathways of the bridged azobenzene derivative presently studied.[17] hν corresponds to irradiation with UV or visible light, and Δ to heating.

Mass-spectrometry-based techniques were already proposed as a powerful characterization tool for the structural characterization of azobenzenes, either alone[18, 19] or in the presence of metals[20, 21] The present work builds on these approaches to gain further information in the kinetics of the complex isomerization processes at work in bridged azobenzenes. On the one hand, we used on-line LC-UV-MS to study the kinetics of the *E*→*Z* thermal back relaxation, and particularly focused on the influence of the solvent on both the kinetics and the steady-state *Z1*/*Z2* ratio formation. However, LC-UV-MS was compatible with the timescale of the isomerization reactions only at low temperatures. Typically, kinetics with timescales shorter than one minute are not accessible by LC. In such cases, the isomerization kinetics were monitored through ion mobility mass spectrometry (IMS-MS) measurements, which proved adapted to timescales down to seconds.[22] In the following, we show that the combination of LC-UV and IMS-MS approaches allows the characterization of relaxation kinetics on a temperature range broad enough to estimate the associated activation energies in different solvents.

METHODOLOGY

Chemicals and materials. Bridged azobenzene isomers were synthetized following the previously published synthesis.[17] *Z1* and *Z2* isomers were isolated by flash chromatography and analyzed by mass spectrometry (MS). *E* isomer was analyzed from a mixture containing *Z1/Z2/E* in an approximate initial ratio 20/10/70, as the *E* isomer at 10 to 100 μmol L^{-1} cannot be isolated and

stored. Ultrapure water was produced using a Milli-Q water purification system (Merck Millipore). Propan-2-ol, acetonitrile and all the metallic salts were purchased from Sigma-Aldrich (Saint-Quentin Fallavier, France), whereas cyclohexane, ethyl acetate, methanol and ethanol were purchased from VWR (Fontenay-sous-Bois, France).

LC-UV-MS experiments. The mixture of the three isomers (*Z1*, *Z2* and *E*) was separated online using a 1260 series Agilent system packed with a X-bridge reversed phase column (Kinetex XB-C18 100 * 3 mm * 2.6 µm) coupled to a mass spectrometer (AmaZon speed ETD, Bruker) operating in the positive ionization mode. LC conditions were as follows: solvent A H_2O + 5 % acetonitrile, solvent B acetonitrile + 5 % H_2O, flow rate 400 µL min^{-1}, injection volume 5 µL of a mixture containing *Z1/Z2/E* in an approximate initial ratio 20/10/70, column temperature 30 °C, elution gradient: 0 min (60 % A), 5 min (25 % A), 7 min (25 % A), 8 min (60 % A) UV detection: 232 nm. Separation was achieved in less than 6 minutes, resulting in a total run time of 12 minutes including reconditioning.

TWIMS-MS experiments. The traveling wave ion mobility mass spectrometry (TWIMS-MS) instrument (Synapt G2-Si HDMS, Waters) was equipped with an ESI source operating in the positive ionization mode. Source conditions were optimized in order to reduce "in source" isomerization of azobenzene compounds, notably by decreasing the sampling cone voltage and the source temperature. The following parameters were chosen: capillary voltage 2.5 kV, sampling cone 30 V and source temperature 50°C. Samples of pure *Z1* and *Z2* isomers, prepared at a final concentration of 10 µmol L^{-1} in MeOH with different metallic salts were analyzed by direct infusion. Optimized ion mobility parameters using $AgNO_3$ salt and N_2 as buffer gas are the following: wave velocity 800 m s^{-1}, wave height 40 V, and gas flow 90 mL min^{-1}. For kinetic studies, a mixture containing *Z1/Z2/E* in an approximate initial ratio 20/10/70 was

infused in the ESI source with a syringe at a flow rate of 350 µL h^{-1}. The syringe temperature was adjusted using a pipe plugged to a thermostated water bath flowing at approximately 40 mL min^{-1}. For on-line LC-TWIMS-MS, Acquity I-class chromatograph was used with identical LC conditions as those described in the LC-UV-MS experimental part.

DTIMS-MS experiments. Homemade drift tube ion mobility instrument (DTIMS-MS) previously described,[23] and equipped with two 79 cm long drift tubes filled with helium (4 Torr),was used to determine experimental collision cross sections (CCS). To this end, arrival times were recorded at different drift voltages. The cross sections were extracted from the linear dependence of the arrival time to the inverse drift voltage, based on the Mason-Schamp equation.[24] In order to isolate $[E+Ag]^+$ species, a 1260 series Agilent system packed with a X-bridge reversed phase column (Kinetex XB-C18 100 * 3 mm * 2.6 µm) was coupled online to the IMS-MS instrument. LC conditions were changed in order to obtain broader peaks, adapted to the DTIMS analysis time scale. The following settings were used: solvent A: $AgNO_3$ 20 µmol L^{-1} in H_2O, solvent B: $AgNO_3$ 20 µmol L^{-1} in acetonitrile, flow rate 500 µL min^{-1}, injection volume 10 µL of a *Z1/Z2/E* mixture, isocratic elution of 8 minutes containing 38 % of the aqueous phase.

IRMPD action spectroscopy experiments. InfraRed Multiple Photon Dissociation (IRMPD) spectra were obtained by using the beamline of the free electron laser (FEL) of the Centre Laser Infrarouge d'Orsay (CLIO).[25] The electron energy of the FEL was set at 41.5 MeV to optimize the laser power in the frequency region of interest (700-1700 cm^{-1}). The FEL beamline was coupled to an experimental platform based on a modified Bruker Esquire 3000+ quadrupole ion trap, which has been already described in details.[26, 27] A 2 mm tapered hole is drilled in the annular electrode of the quadrupole ion trap to allow access of the IR laser to the center of the trap. Multistage mass spectrometry was carried out using the standard Bruker Esquire Control

(v5.2) software, and mass-selected ions were irradiated (typical irradiation time 180-250 ms) using the MS^2 step, where the excitation amplitude was set to 0 to avoid any CID-like process. Mass spectra were recorded after 10 accumulations, using the standard mass range (*m/z* 50-3000) and the normal scan resolution (13000 Th/s), the accumulation time being typically of 20 ms. This sequence was repeated ten times for each photon energy.

IRMPD spectra are obtained by plotting the photofragmentation yield R (equation 1)

$$R = -\ln[I_{precursor}/(I_{precursor} + \Sigma I_{fragments})] \quad (1)$$

(where $I_{precursor}$ and $I_{fragments}$ are the integrated intensities of the mass peaks of the precursor and of the fragment ions, respectively) as a function of the frequency of the IR radiation. Spectra were externally calibrated in energy using polystyrene as reference in the 700 to 1700 cm^{-1} range.

DFT calculations. DFT calculations were carried out using B3LYP functional, as implemented in the Gaussian-09 set of programs.[28] B3LYP combines the non-local correlation function of Lee, Yang and Parr,[29] with the Becke's three-parameter non local hybrid exchange functional.[30] The different structures were optimized with the dp-polarized 6-31G(d,p) basis set for C, H, N and O atoms, without any symmetry constraint. Harmonic vibrational frequencies were estimated at this level to classify the stationary points either as local minima or transition states , and to estimate the zero-point vibrational energy (ZPVE) corrections. For Ag, we used the relativistic effective core potential (RECP) developed by Hay and Wadt (LANL2DZ).[31] This RECP include the outermost core orbitals 4s and 4p in the valence shell. The valence basis set is a [3s3p2d] contraction of a (5s6p4d) primitive set of Hay and Wadt. With regard to band positions, a scaling factor of 0.965 was chosen on the basis of the overall good agreement between experimental and computed frequencies. Finally, for a better comparison with the experimental IRMPD signal, computed spectra were convoluted with a 15 cm^{-1} Lorentzian function.

The MOBCAL software[32, 33] was used to convert cartesian coordinates in CCS values. Lennard-Jones parameters for silver were based on the scaled Universal Force Field for Helium (2.5184 Å, 1.249 meV).[34, 35]

RESULTS AND DISCUSSION

In a preliminary work, we tried to determine whether tandem mass spectrometry could achieve isomeric distinction through the formation of isomer-specific fragment ions. To this end, we performed MS/MS experiments on ions arising from different cationizing agents, such as proton, alkali, alkali-earth, transition metals or heavy metals. As the unstable *E* isomer cannot be isolated pure, LC separation of a *Z1/Z2/E* mixture was performed to characterize the MS/MS pattern of each independent azobenzene isomer, the metal salt being added to the aqueous mobile phase. Depending on the ionizing agent, different types of ions were generated by electrospray (see Table S1 and Figures S1 to S6 of the Supporting Information). Protonation of the different azobenzene isomers results in the formation of intense $[M+H]^+$ and $[2M+H]^+$ ions in the gas phase, which exhibit similar MS/MS spectra (Figure S1). Use of alkali salts lead to the systematic formation of $[M+Alk]^+$ and $[2M+Alk]^+$ complexes. Similar ions are generated in presence of Ag^+ (Figure S2) and Cu^{2+} salts (which resulted in Cu(I) complexes under our experimental conditions) with again, no isomeric distinction (Figure S3). When using Mn^{2+} and alkali-earth metals, different doubly-charged complexes could be observed, depending on the isomer; the *Z1* isomer mostly gives rise to $[4Z1+Cat]^{2+}$ complexes, whereas the *Z2* isomer interacts to generate a prominent trimeric $[3Z2+Cat]^{2+}$ ions. On the other hand, no complexes were detected with the *E* isomer (Figure S4). Concerning the remaining transition metals, it is worth noting that the discrimination of the three isomers could be achieved on ESI-MS spectra for Zn^{2+}, Fe^{2+} and Co^{2+} (Figures S5 and S6).

To summarize, tandem mass spectrometry did not allow an easy differentiation of *Z1*, *Z2* and *E* isomers in mixture. In spite of the different nature of the complexes generated, MS^2 and MS^n spectra turned to be similar for the azobenzene isomers. Even if isomer-specific complexes could be identified by LC-MS experiments (*i.e.* using Zn^{2+}, Co^{2+} and Fe^{2+}), the intensities of the associated ions for both *E* and *Z2* were too low to allow quantitation (Figures S5 and S6) of the different compounds in mixture. We also considered the possibility to generate radical cations of azobenzenes through the fragmentation of ternary complexes. To this end, different types of auxiliary ligands were considered in combination with Cu^{2+} or Zn^{2+} (arginine, phenylalanine, serine, 1,10-phenatroline, ethylenediamine, terpyridine, 12-crown-4 and bipyridine). The ternary complexes generated did not display specific CID fragmentation. Azobenzene radical cations $M^{+\bullet}$ could only be generated from the dissociation of $[Cu(M)(ethylediamine)]^{2+}$ complex, but their fragmentation did not allow any isomeric distinction. Therefore, an upstream separation dimension to UV and MS was mandatory to characterize each isomer. Two different separation techniques were then considered, allowing analysis at different timescales: liquid chromatography (minute timescale) and ion mobility spectrometry (millisecond timescale).

On-line LC-UV-MS .

On-line LC-UV-MS experiments were first performed to characterize each isomer. Reversed phase liquid chromatography allowed the separation of the three isomers in less than six minutes (Figure 1). Moreover, UV detection permitted the different isomers to be quantified. Note that precise quantification based on MS signals could not be achieved because the protonated forms of the different isomers exhibit different stabilities. As a matter of fact, upon CID, the $[Z2+H]^+$ ion undergoes less fragmentation the *Z1* and *E* counterparts, regardless both the elution gradient and the cationized species used. Consequently, the proportion of each isomer in mixture cannot

be determined using MS detection, and therefore the kinetic study of *E*→*Z* isomerization was investigated by coupling LC to UV detection.

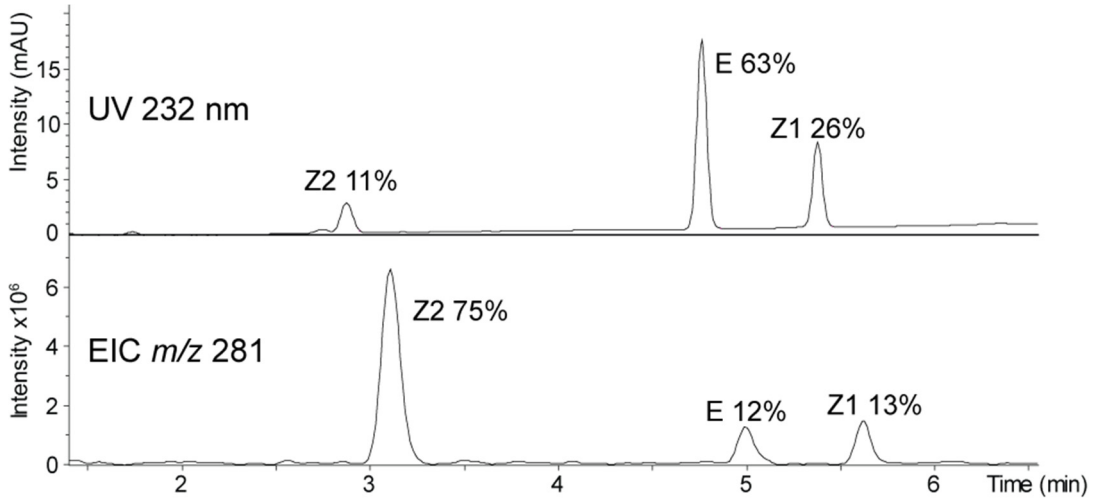

Figure 1. UV trace at 232 nm (top) and extracted ion chromatogram (EIC) of $[M+H]^+$ at *m/z* 281 (bottom) obtained after LC separation of a mixture containing *Z1/Z2/E* in 26/11/63 ratio infused in MeOH at 30°C.

Due to the slow thermal back relaxation of *E*→*Z* isomers, the temperature was adjusted in the autosampler at 30 and/or 40°C. In addition, different dilution solvents were used to study their effect on *E*→*Z* isomerization (Table 1 and Figures S7 and S8). In this case, thermal back relaxation occurs in the vial and allows the use of solvents which are not compatible with UV detection, as the azobenzene will be diluted and eluted in the mobile phase of the column.

First order reaction kinetics of *E*→*Z* thermal back relaxation can be expressed as:

$$[E] = [E_0]\exp(-kt) \qquad (2)$$

, where [*E*] is the concentration of *E* at time *t*, [*E0*] is the initial concentration and *k* is the reaction rate coefficient. Due to potential *E*→*Z* isomerization that may occur during the desolvation process, the population observed for isomer E may be only a fraction of the actual population in solution. However, it can be assumed that the fraction of the initial *E* population which converts to Z in source is not affected by the temperature of the solution. Under this

hypothesis, the time-evolution of the observed population of the E isomer, is expected to follow equation 2 except for a multiplicative constant, which does not affect the value of the kinetic constant that can be extracted. This is indeed supported by the observation that the time evolution of *E* can be well reproduced assuming a single exponential decay. The data obtained for the time evolution of the relative concentrations of *E vs Z1/Z2,* determined from UV peaks area, are reported in Figure S9 and S10 in different solvents at different temperatures (Supporting Information). By fitting the data based on equation 1, the kinetic rate constants for *E*→*Z* thermal back relaxation were determined in each case, and are listed in Table 1.

Table 1. Relaxation time of *E*→*Z* isomerization and final proportions of *Z1/Z2* isomers as determined by on-line LC-UV experiments using different solvents and temperatures.

Solvent	Temperature (°C)	$k_{(E\rightarrow Z)}$ (h^{-1})	$1/k_{(E\rightarrow Z)}$ (h)	Z1/Z2
Cyclohexane	40	1.51	0.66	70/30
Ethyl acetate	40	1.36	0.73	69/31
Propan-2-ol	30	0.32	3.08	65/35
	40	0.90	1.11	65/35
Ethanol	40	0.82	1.22	60/40
Acetonitrile	30	0.22	4.45	57/43
	40	0.65	1.55	57/43
Methanol	30	0.20	4.94	56/44
	40	0.61	1.63	56/44
Water	30	0.06	16.12	18/82
	40	0.20	5.04	16/84

From Table 1, we can observe that increasing the temperature significantly increases the rate of the *E*→*Z* thermal back relaxation. As a matter of fact, for the different solvents studied at different temperatures, the rate of isomerization is three times faster when the temperature increases by 10°C. The most significant example is obtained by using purified water. In that case, the relaxation time decreased from 16 hours at 30°C to 5 hours at 40°C (Table 1). Surprisingly, for a given solvent, the final *Z1/Z2* ratio, which reflects the populations at equilibrium, does not depend on temperature. This suggests that within the temperature range

explored, the relative entropy and enthalpy changes associated with the two considered isomerization pathways, remain unchanged. On the other hand, data show that the nature of the solvent dramatically influences both the kinetics and the equilibrium populations. As a matter of fact for a given temperature, increasing the solvent polarity mostly results in longer relaxation times. In addition, it also favors the *E*→*Z2* isomerization pathways over the *E*→*Z1* isomerization (e.g. the equilibrium *Z1/Z2* ratio is 70/30 in cyclohexane and 16/84 in water). This latter effect might be explained by a more pronounced affinity of polar solvents for the acetal moiety of the *E* isomer. The resulting steric hindrance would then favor the folding of phenyl groups at the opposite of the acetal bridge, leading to the preferred formation of the *Z2* isomer.

IMS-MS and IRMPD measurements

In order to study the of *E*→*Z* isomerization process at higher temperatures, we have used ion mobility-mass spectrometry, which allows isomer separation on a shorter time scale (millisecond), and therefore the monitoring of faster isomerization reactions.

Isomer separation by IMS-MS

An extensive screening of ionizing agents (alkali, alkaline earth and transition metals) has been performed in order to differentiate *Z* isomers in the IMS dimension (data not shown). It turned out that baseline separation of *Z* isomers has only been achieved with silver cations, by considering $[M+Ag]^+$ species (Figure 2). From these data, it is worth mentioning that both *Z1* and *Z2* isomers displayed two peaks, unlike when analysed in the drift tube instrument (Figure S11). It has to be noted that the conditions are softer in the latter instrument. Consequently, the presence of signal at a drift time corresponding to that of *Z1* within the arrival time distribution

(ATD) recorded for *Z2*, and *vice versa*, in the TWIMS ATD can be attributed to Z1/Z2 isomerization occurring either in source, or during the separation.

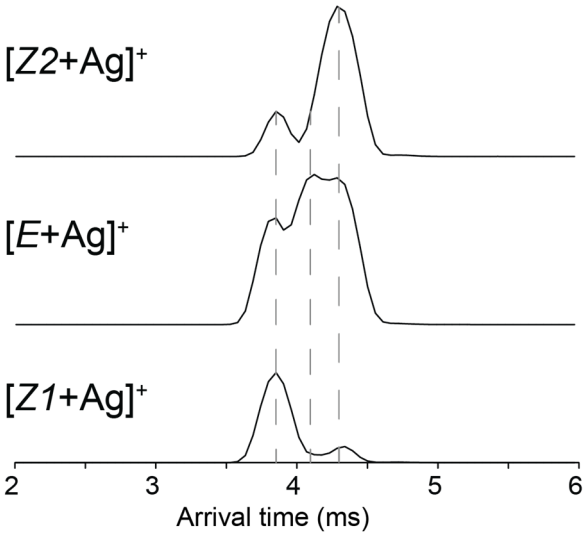

Figure 2. Extracted arrival time distributions of $[M+Ag]^+$ ion (*m/z* 387.0) obtained from traveling wave ion mobility after LC separation of a mixture of *Z1/Z2/E* isomers in 25/10/65 ratio. Intensities of *Z1* and *Z2* isomers are relative to the *E* isomer intensities.

LC-IMS-MS experiments were then used to determine the IMS profile of the *E* isomer which cannot be isolated off-line due to its instability. Unfortunately, it was not possible to record a drift tube ATD for *E*, due to the incompatibility of the duty cycle of the drift tube with LC separation times. As visible on Figure 2, the ATD for $[E+Ag]^+$ ions displayed a broad peak. Three barely-resolved populations can be distinguished in this ATD, based on the expected peak that can be inferred from the signal obtained from Z1 or Z2 (Figure S12). Among those three populations, the ones centered at the drift times measured at 3.6 and 4.3 ms are attributed to ions which have undergone isomerization to $[Z1+Ag]^+$ and $[Z2+Ag]^+$, respectively. Their relative position is also consistent with the drift tube ATDs obtained for the two species, which further supports the above assignation. The central feature, at 4.1 ms is then attributed to the remaining *E* population.

Structural characterization of [Z+Ag]⁺ isomers.

In order to confirm the assignment of *Z1* and *Z2* isomers for silver-cationized species and understand the differences observed from IMS-MS experiments, we combined different experimental and theoretical approaches. We first used IRMPD action spectroscopy to study the structure of the $[Z+Ag]^+$ ions. Since the IRMPD time scale was not compatible with LC, IRMPD spectra of $[E+Ag]^+$ isomer could not be recorded experimentally.

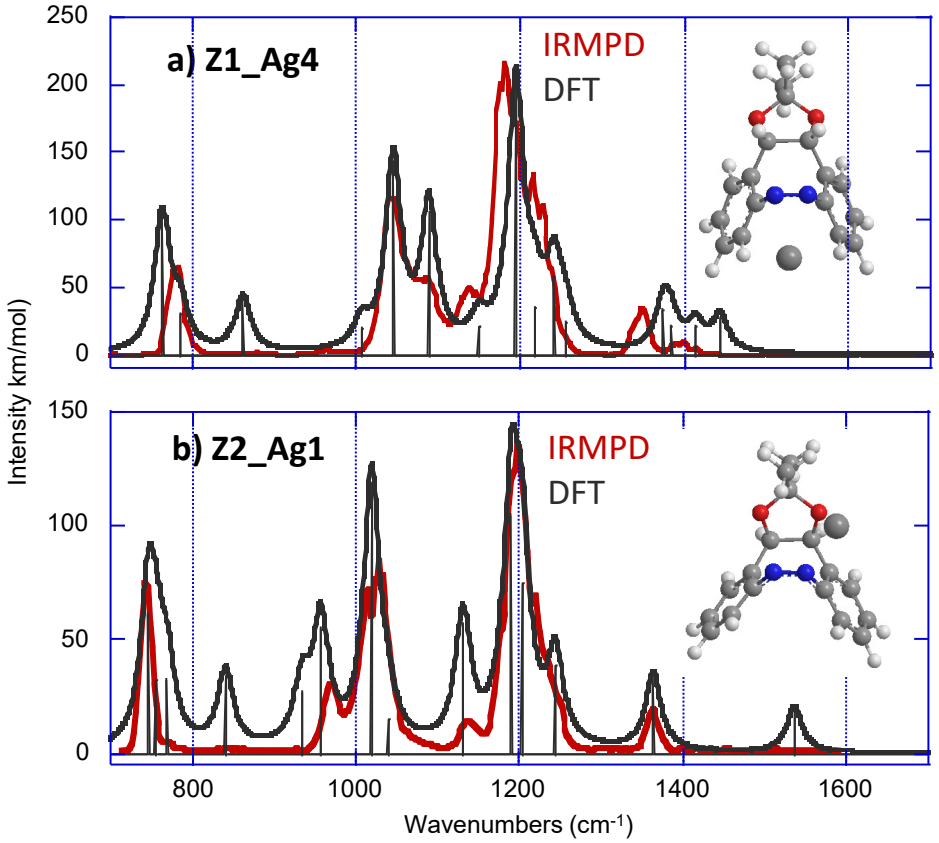

Figure 3. Overlay of experimental (in red) and theoretical (in black) IRMPD action spectroscopy spectra of a) $[Z1+Ag]^+$ and b) $[Z2+Ag]^+$ isomers.

The IRMPD spectra obtained for $[Z1+Ag]^+$ and $[Z2+Ag]^+$ complexes are gathered in Figure 3. For both complexes, similar photo-fragments were observed, which correspond to the loss of acetone (58 u) and elimination of AgH (108/110 u). As shown in Figure 3, these two experimental IRMPD spectra share similarities: a major feature around 1200 cm^{-1}, an intense

band below 800 cm^{-1}, two weak absorptions around 1140 and 1350 cm^{-1} and finally a combination of two bands detected between 960 and 1100 cm^{-1}. However, one can observe that the position of several bands differs significantly, suggesting that the two complexes are associated with different binding schemes.

Structural assignment by IRMPD is based on the comparison of the experimental trace with the spectra computed for the low energy-lying structures. The different structures optimized for *Z1* and *Z2* complexes are given in the Supporting Information (Figure S13), whereas for each ion, the experimental IRMPD spectrum is overlaid in Figure 3 with the vibrational IR spectrum computed for the most stable structure of $[Z1+Ag]^+$ and $[Z2+Ag]^+$ complexes, namely **Z1_Ag4** and **Z2_Ag1**, respectively. First, if one considers the *Z1* isomer, the harmonic IR spectrum (black) computed for **Z1_Ag4**, is globally in good agreement with the experimental data (red). This structure is characterized by a silver atom located in between the two benzenic rings. Other binding schemes have been optimized but result in less stable structures (Figure S13). Almost all the IRMPD bands can be assigned by considering the IR active modes of **Z1_Ag4**, which are detailed in Table S2 (Supporting Information).

Considering the $[Z2+Ag]^+$ complex, the acetal moiety is now in *cis* position with respect to the N=N bridge, thereby allowing the simultaneous interaction of the metallic center with both an oxygen and a nitrogen atom. This binding mode corresponds to the **Z2_Ag1** form, which is the global minimum obtained during this study. As compared to neutral forms of *Z1* and *Z2* which are practically degenerate,[17] **Z2_Ag1** is 20.2 $kJ.mol^{-1}$ more stable than **Z1_Ag4**, due to a different binding scheme, and is also more stable than **Z2_Ag2**, the counterpart of the most stable form obtained for *Z1*. Note that we obtained only two stable geometries, all other attempts evolving towards **Z2_Ag1** during geometry optimization. Examination of Figure 3 shows a very good agreement between the experimental IRMPD spectrum of $[Z2+Ag]^+$, and the vibrational spectrum computed for **Z2_Ag1**. The C-O stretch attributed to the band detected at

1085 cm^{-1} for **Z1_Ag4** is red-shifted for **Z2_Ag1** (1025 cm^{-1}), as the result of the interaction of the silver atom with one oxygen atom of the acetal moiety. Note also that due to silver complexation, the central CNNC moiety within **Z2_Ag1** is slightly more distorted (2.6°) as compared to the neutral crystal structure (0.6°).[17] The effect is much less pronounced for **Z1_Ag4**, the CNNC moiety being planar (0.02°). NNC angles are smaller for (118.5-118.6°) for **Z1_Ag4** than for **Z2_Ag1** (119.7-123.6°), as the result of the interaction of Ag^+ with the two phenyl rings for the former.

Collision cross section measurements

In addition to IRMPD experiments, we also determined by drift tube ion mobility experiments the collision cross section (CCS) of *Z* isomers. Results are reported in Tables 2 and S4. These experiments confirmed that $[Z1+Ag]^+$ adopted a more folded gas-phase conformation than $[Z2+Ag]^+$ (Figure S13, Table 2). The theoretical CCS values computed for the most stable forms for each isomer, **Z1_Ag4** and **Z2_Ag1**, are consistent with a more folded gas-phase conformation for $[Z1+Ag]^+$ compared to $[Z2+Ag]^+$. However, absolute values differ by more than 10% from experimental CCS values. Such important differences can be ascribed to the lack of silver parametrization in the MOBCAL software as we used the procedure described by Lalli *et al*, initially developed for anions.

Table 2. Experimental CCS values obtained from drift tube ion mobility experiments, and theoretical CCS values obtained with the trajectory method algorithm of MOBCAL on the lowest energy structure determined by DFT calculations.

	CCS_{Exp}	CCS_{Theo}
Z1 (Z1_Ag4)	106 ± 2 Å²	96.3 Å²
Z2 (Z2_Ag1)	115 ± 2 Å²	97.1 Å²

In summary, the combination of IRMPD and ion mobility data tends to retain **Z1_Ag4** and **Z2_Ag1** as the probable structures for [*Z1*+Ag]$^+$ and [*Z2*+Ag]$^+$ complexes, respectively.

Kinetic study from IMS-MS experiments

The unambiguous characterization of silver azobenzene cations allows performing the *E*→*Z* kinetic study using IMS-MS analysis. Quantitation by ion mobility of the *E/Z* ratio in mixture can be achieved by using the [M+Ag]$^+$ signals. This ratio is deduced from the peak area (obtained after a gaussian fit, Figure S12) of the signal at 4.0 ms for the *E* isomer, and the peaks area of signals at 3.6 and 4.3 ms corresponding to *Z* isomers. We previously showed that *E*→*Z* "in-source" isomerization occurs during TWIMS experiments (Figure 2) and depends on MS parameters. For kinetic studies, all the instrument parameters (voltages, temperatures and drift conditions) were kept unchanged. Then, potential isomerization taking place in-source, or during the separation, would result in a constant change in the observed population ratio, independent of time and on the temperature of the solution. Under these conditions, any change in the population ratio as a function can be attributed to isomerization in solution.

Due to the different ionization yields observed for *Z1* and *Z2* in function of the MS-compatible solvent used (Figure 4), *E*→*Z1* and *E*→*Z2* isomerization kinetics could not be quantitatively determined even when calibration curves (using different known ratios of *Z1/Z2*) were performed. Note that we did not try to exploit the relative steady-state intensities of the *Z1* and *Z2* isomers measured by IMS. Large variations were observed when comparing the final ratio obtained from UV measurements to those from IMS using different solvents. We interpret these variations as the result of dramatic changes in the relative ionization efficiency of the two isomers depending on the solvent. Fortunately, this effect does not affect the measured kinetic rate constants, since only the rate of the intensity change is exploited.

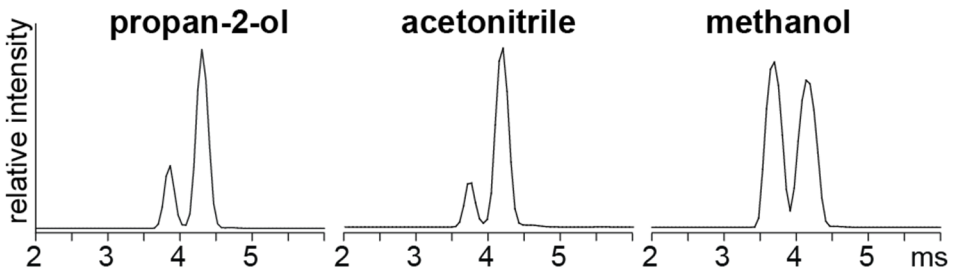

Figure 4. Extracted traveling wave ion mobility spectra of an equimolar mixture of *Z1/Z2* isomers as $[Z+Ag]^+$ ions in propan-2-ol, acetonitrile and methanol.

It is worth noting that dimers $[2E+Ag]^+$ species were also observed in the MS spectra and could be easily quantified from TWIMS experiments as its conformation was significantly more folded than *Z* silver $[2Z+Ag]^+$ dimers.[36] We confirmed that IMS peaks area ratio of $[E+Ag]^+/[2E+Ag]^+$ is constant for propan-2-ol and methanol, and slightly decreases for acetonitrile in function of the time, and therefore does not influence the $E \rightarrow Z$ kinetic determination from IMS-MS experiments (Figure S16).

In order to perform the kinetic study, an azobenzene mixture of *Z1/Z2/E* in an approximate initial ratio of 20/10/70 was heated in the injection syringe, by using the homemade heating system described in the experimental section. As the mixture was prepared at 20°C to slow down isomerization prior to IMS-MS experiments, an equilibration time of 5 minutes was required for the azobenzene mixture to reach the syringe temperature. Consequently, data recorded at the beginning of the kinetic were not considered to estimate the $E \rightarrow Z$ relaxation time (Figures S17 to S19) for the different experimental conditions (Table 3).

Table 3. Relaxation time associated to $E \rightarrow Z$ isomerization determined by IMS-MS experiments, using different solvents and temperatures.

Solvent	Temperature (°C)	$k_{(E \rightarrow Z)}$ (h^{-1})	$1/k_{(E \rightarrow Z)}$ (min)
Propan-2-ol	50	1.83	32.8
	60	6.30	9.5
	70	12.24	4.9
Acetonitrile	50	2.03	29.6
	60	5.26	11.4
	70	10.26	5.8
Methanol	50	1.74	34.6
	60	4.83	12.4

For the different solvents studied, results obtained with TWIMS-MS at 50, 60 and 70°C show a rate constant increase by a factor of three ongoing from 50 to 60°C, and an additional factor of two from 60 to 70°C in the particular case of propan-2-ol and acetonitrile, these latters allowing higher temperatures due to their higher boiling points. Similarly to results obtained by LC-UV, the rate constants observed in propan-2-ol are globally higher than those obtained in acetonitrile**.**

The activation energies associated with the $E \rightarrow Z$ isomerization can be estimated from the Arrhenius law:

$$k = A \exp(-E_a/RT) \qquad (3)$$

, where A is the frequency factor, E_a the activation energy, R the ideal gas constant and T the absolute temperature. The activation energy can be deduced from the plot ln k in function of $1/RT$ with a slope equal to $-E_a$ (Figure 5). From these plots, showing regression coefficients higher than 0.99**,** activation energies associated with the of $E \rightarrow Z$ isomerization were determined for methanol (88.5 kJ mol^{-1}), acetonitrile (84.3 kJ mol^{-1}) and propan-2-ol (79.6 kJ mol^{-1}). Note that similar rate constants were determined at 40°C using either IMS-MS or LC-UV techniques (Figure S20).

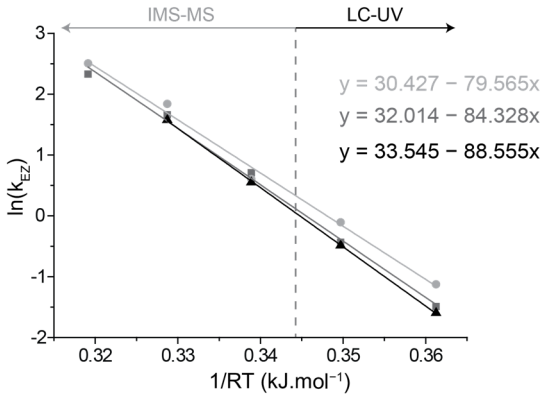

Figure 5. Arrhenius plots ln k_{EZ} = f (1/RT) obtained by LC-UV (30 and 40 °C) and TWIMS-MS (50, 60 and 70 °C) for different solvents: methanol in black triangles, acetonitrile in dark grey squares and propan-2-ol in light grey circles.

Therefore, although rather small, these differences in the activation energies observed can result in very significant solvent effects, especially at low temperatures. These activation energies might also be helpful for a better understanding of the photochemistry occurring in different solvents for this uncommon three-species photoswitching system.

CONCLUSION

We used LC-UV and IMS-MS to characterize the thermal back relaxation in a three-states photoswitchable azobenzene. The combination of these techniques appears as a good complement to UV-Vis absorption spectroscopy in this context. In particular, the sensitivity and specificity of mass spectrometry could be an advantage for the characterization of such species when present in low abundance or in complex mixtures. From LC-UV experiments, relaxation times could be easily determined at low temperature, and effect on isomerization can be observed for various solvents. We could observe that the rates of $E \rightarrow Z$ thermal back relaxation increased when both the solvent polarity and the temperature increased. Moreover, the solvent

polarity also influences the *E*→*Z1* and *E*→*Z2* ratio. *Z2* formation is indeed favored with polar solvents whereas *Z1* is preferred for non-polar solvents.

Isomer separation could be achieved by IMS-MS experiments through Ag^+ complexation, thereby allowing the determination of *E*→*Z* relaxation rate constants at higher temperatures than LC-UV experiments. Based upon the combination of IRMPD-MS and DTIMS-MS experiments, silver complexation in the gas phase leading to $[Z1+Ag]^+$ and $[Z2+Ag]^+$ ions, is associated with location of the silver cation between the two phenyl rings for *Z1,* and between N and O heteroatoms for *Z2*. The combination of both LC-UV and IMS-MS experiments allows the determination of *E*→*Z* isomerization rate constant at different temperatures, and consequently the estimates of associated activation energies in different solvents. We could notably estimate that the energy barrier for *E*→*Z* isomerization is almost 10 kJ mol^{-1} higher in methanol than in propan-2-ol, pointing up the important solvent influence, especially at low temperatures.

CONFLICTS OF INTEREST

The authors declare no competing financial interest.

ACKNOWLEDGMENT

JYS and SP gratefully acknowledge the aid and expertise of the CLIO facility support staff, Debora Scuderi, Vincent Steinmetz and Philippe Maitre. They also warmly acknowledge Dr. Alan Morin for his help in designing the syringe heating system.

This work is supported by a public grant overseen by the French National Research Agency (ANR) as part of the "Investissements d'Avenir" program (Labex Charmmmat, reference: ANR-11-LABX-0039-grant)

AUTHOR INFORMATION

Corresponding Authors

* E-mail: salome.poyer@cnrs.fr, tel : +33 (0)1 69 82 45 87

* E-mail: jeanyves.salpin@univ-evry.fr, tel: +33 (0)1 69 47 76 44

REFERENCES

1. S. E. Braslavsky, *Pure Appl. Chem.*, 2007, **79**, 293.
2. W. Szymanski, J. M. Beierle, H. A. Kistemaker, W. A. Velema and B. L. Feringa, *Chem. Rev.*, 2013, **113**, 6114-6178.
3. J. Broichhagen, J. A. Frank and D. Trauner, *Acc. Chem. Res.*, 2015, **48**, 1947-1960.
4. M. M. Lerch and M. J. Hansen, *Angew. Chem. Int. Ed. Engl.*, 2016, **55**, 10978-10999.
5. M. Vlatković, B. S. L. Collins and B. L. Feringa, *Chem. Eur. J.*, 2016, **22**, 17080-17111.
6. V. Blanco, D. A. Leigh and V. Marcos, *Chem. Soc. Rev.*, 2015, **44**, 5341-5370.
7. R. Gostl, A. Senf and S. Hecht, *Chem. Soc. Rev.*, 2014, **43**, 1982-1996.
8. M. Kathan and S. Hecht, *Chem. Soc. Rev.*, 2017, **46**, 5536-5550.
9. A. Diaz-Moscoso and P. Ballester, *Chem. Commun.*, 2017, **53**, 4635-4652.
10. Z. Yu and S. Hecht, *Chem. Commun.*, 2016, **52**, 6639-6653.
11. A. J. McConnell, C. S. Wood, P. P. Neelakandan and J. R. Nitschke, *Chem. Rev.*, 2015, **115**, 7729-7793.
12. E. Leonard, F. Mangin, C. Villette, M. Billamboz and C. Len, *Cat. Sci. Tech.*, 2016, **6**, 379-398.
13. M. Dong, A. Babalhavaeji, S. Samanta, A. A. Beharry and G. A. Woolley, *Acc. Chem. Res.*, 2015, **48**, 2662-2670.
14. A. A. Beharry and G. A. Woolley, *Chem. Soc. Rev.*, 2011, **40**, 4422-4437.
15. H. M. Bandara and S. C. Burdette, *Chem. Soc. Rev.*, 2012, **41**, 1809-1825.
16. R. Siewertsen, H. Neumann, B. Buchheim-Stehn, R. Herges, C. Nather, F. Renth and F. Temps, *J. Am. Chem. Soc.*, 2009, **131**, 15594-15595.
17. C. Deo, N. Bogliotti, R. Métivier, P. Retailleau and J. Xie, *Chem. Eur. J.*, 2016, **22**, 9092-9096.
18. L.-H. He, G.-M. Wang, Q. Tang, X.-k. Fu and C.-B. Gong, *J. Mat. Chem. C*, 2014, **2**, 8162-8169.
19. L. H. Urner, M. Schulze, Y. B. Maier, W. Hoffmann, S. Warnke, I. Liko, K. Folmert, C. Manz, C. V. Robinson, R. Haag and K. Pagel, *Chem. Sci.*, 2020, **11**, 3538-3546.
20. T. Yutaka, I. Mori, M. Kurihara, J. Mizutani, K. Kubo, S. Furusho, K. Matsumura, N. Tamai and H. Nishihara, *Inorg. Chem.*, 2001, **40**, 4986-4995.
21. M. Juribašić, A. Budimir, S. Kazazić and M. Curić, *Inorg. Chem.*, 2013, **52**, 12749-12757.
22. T. Wyttenbach, N. A. Pierson, D. E. Clemmer and M. T. Bowers, *Ann. Rev. Phys. Chem.*, 2014, **65**, 175-196.
23. A.-L. Simon, F. Chirot, C. M. Choi, C. Clavier, M. Barbaire, J. Maurelli, X. Dagany, L. MacAleese and P. Dugourd, *Rev. Sci. Instrum.*, 2015, **86**, 094101.
24. H. E. Revercomb and E. A. Mason, *Anal. Chem.*, 1975, **47**, 970-983.
25. R. Prazeres, F. Glotin, C. Insa, D. A. Jaroszynski and J. M. Ortega, *Eur. Phys. J. D*, 1998, **3**, 87-93.
26. L. Macaleese, A. Simon, T. B. Mcmahon, J. M. Ortega, D. Scuderi, J. Lemaire and P. Maître, *Int. J. Mass Spectrom.*, 2006, **249/250**, 14-20.
27. A. Simon, L. Macaleese, P. Maitre, J. Lemaire and T. B. McMahon, *J. Am. Chem. Soc.*, 2007, **129**, 2829-2840.
28. M. J. Frisch et al., *see supporting information for complete citation for the Gaussian code of programs*.
29. C. Lee, W. Yang and R. Parr, *Phys. Rev. B*, 1988, **37**, 785-789.
30. A. D. Becke, *J. Chem. Phys.*, 1993, **98**, 5648-5652.
31. P. J. Hay and W. R. Wadt, *J. Chem. Phys.*, 1985, **82**, 299-310.
32. M. F. Mesleh, J. M. Hunter, A. A. Shvartsburg, G. C. Schatz and M. F. Jarrold, *J. Phys. Chem.*, 1996, **100**, 16082-16086.
33. A. A. Shvartsburg and M. F. Jarrold, *Chem. Phys. Lett.*, 1996, **261**, 86-91.
34. A. K. Rappe, C. J. Casewit, K. S. Colwell, W. A. Goddard and W. M. Skiff, *J. Am. Chem. Soc.*, 1992, **114**, 10024-10035.
35. P. M. Lalli, Y. E. Corilo, M. Fasciotti, M. F. Riccio, G. F. de Sa, R. J. Daroda, G. H. Souza, M. McCullagh, M. D. Bartberger, M. N. Eberlin and I. D. Campuzano, *J. Mass Spectrom.*, 2013, **48**, 989-997.
36. S. Poyer, C. Comby-Zerbino, C. M. Choi, L. MacAleese, C. Deo, N. Bogliotti, J. Xie, J. Y. Salpin, P. Dugourd and F. Chirot, *Anal. Chem.*, 2017, **89**, 4230-4237.

Kinetic study of azobenzene *E*/*Z* isomerization using ion mobility-mass spectrometry and liquid chromatography-UV detection.

Salomé Poyer[1,2*], Chang Min Choi[3], Claire Deo[4], Nicolas Bogliotti[4], Juan Xie[4], Philippe Dugourd[5], Fabien Chirot[6], Jean-Yves Salpin.[1,2]*

[1] Université Paris-Saclay, Univ Evry, CNRS, LAMBE, Evry-Courcouronnes, 91025, France

[2] CY Cergy Paris Université, CNRS, LAMBE, 95000, Cergy, France

[3] Center for Scientific Instrumentation, Korea Basic Science Institute, Chungbuk, Republic of Korea

[4.] Université Paris-Saclay, ENS Paris-Saclay, CNRS, PPSM, 94235 Cachan, France

[5.] Univ Lyon, Université Claude Bernard Lyon 1, CNRS, UMR5306 Institut Lumière Matière, 69622 Villeurbanne, France

[6.] Univ Lyon, Université Claude Bernard Lyon 1, CNRS, ENS de Lyon, UMR5280 Institut des Sciences Analytiques, 69622 Villeurbanne, France

Supporting information

Complete citation for the Gaussian code of programs

Gaussian 09, Revision C.01,
M. J. Frisch, G. W. Trucks, H. B. Schlegel, G. E. Scuseria, M. A. Robb, J. R. Cheeseman, G. Scalmani, V. Barone, B. Mennucci, G. A. Petersson, H. Nakatsuji, M. Caricato, X. Li, H. P. Hratchian, A. F. Izmaylov, J. Bloino, G. Zheng, J. L. Sonnenberg, M. Hada, M. Ehara, K. Toyota, R. Fukuda, J. Hasegawa, M. Ishida, T. Nakajima, Y. Honda, O. Kitao, H. Nakai, T. Vreven, J. A. Montgomery, Jr., J. E. Peralta, F. Ogliaro, M. Bearpark, J. J. Heyd, E. Brothers, K. N. Kudin, V. N. Staroverov, T. Keith, R. Kobayashi, J. Normand, K. Raghavachari, A. Rendell, J. C. Burant, S. S. Iyengar, J. Tomasi, M. Cossi, N. Rega, J. M. Millam, M. Klene, J. E. Knox, J. B. Cross, V. Bakken, C. Adamo, J. Jaramillo, R. Gomperts, R. E. Stratmann, O. Yazyev, A. J. Austin, R. Cammi, C. Pomelli, J. W. Ochterski, R. L. Martin, K. Morokuma, V. G. Zakrzewski, G. A. Voth, P. Salvador, J. J. Dannenberg, S. Dapprich, A. D. Daniels, O. Farkas, J. B. Foresman, J. V. Ortiz, J. Cioslowski, and D. J. Fox, Gaussian, Inc., Wallingford CT, 2010

Table S1. Nature of the complexes observed with azobenzene under electrospray conditions, in function of the ionizing agent.

Ionizing agent	**Complex generated onto the ESI-MS spectrum**
H^+	$[M+H]^+$, $[2M+H]^+$
Li^+, Na^+, K^+, Rb^+, Cs^+	$[M+Alk]^+$, $[2M+Alk]^+$
Ca^{2+}, Sr^{2+}, Mn^{2+}	$[3M+Cat]^{2+}$, $[4M+Cat]^{2+}$ (M=*Z1*, *Z2*)
Ba^{2+}	$[3M+Ba]^{2+}$(M=E, *Z1*, *Z2*)
	$[4M+Ba]^{2+}$ (M=*Z1*, *Z2*)
	$[5M+Ba]^{2+}$, $[6M+Ba]^{2+}$ (M=*Z1*)
Ag^+, Cu^{2+}	$[M+Cat]^+$, $[2M+Cat]^+$
Ni^{2+}	$[2M+Ni]^{2+}$, $[3M+Ni]^{2+}$, $[4M+Ni]^{2+}$ (M=*Z1*, *Z2*)
Cd^{2+}	$[2M+Cd]^{2+}$, $[3M+Cd]^{2+}$, $[4Z1+Cd]^{2+}$ (M=*Z1*, *Z2*)
Fe^{2+}	$[4Z1+Fe]^{2+}$, $[2(E-58)+Fe]^{2+}$, $[3(Z2-58)+Fe]^{2+}$
Co^{2+}, Zn^{2+}	$[4Z1+Cat]^{2+}$, $[2Z2+Cat]^{2+}$, $[E+Cat]^{2+}$
Fe^{3+}, Ti^{3+}, Au^{3+}, La^{3+}, Eu^{3+}	No complexes

Figure S1. CID MS/MS spectra observed for a) $[Z2+H]^+$, b) $[E+H]^+$ and c) $[Z1+H]^+$.

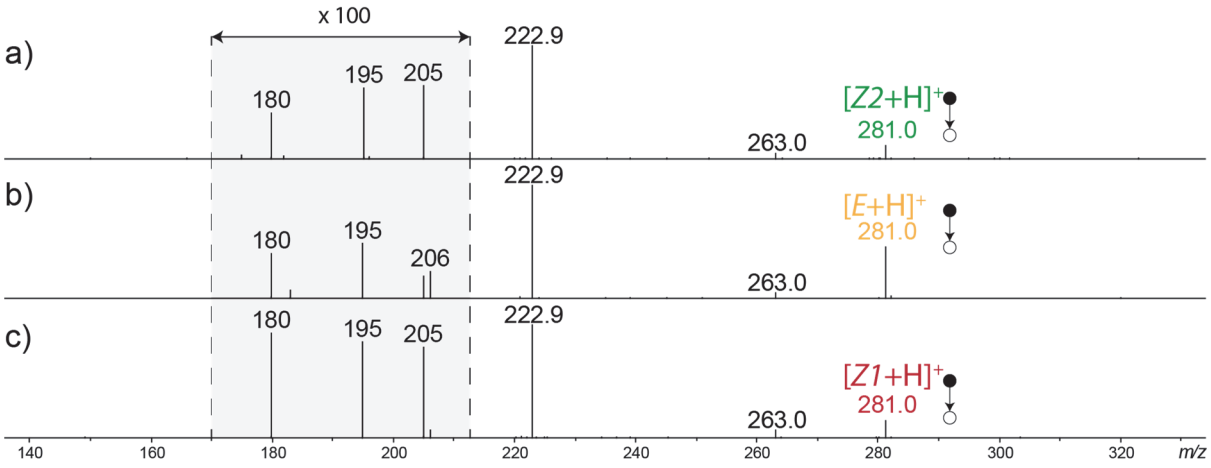

Figure S2. MS spectra observed for a) *Z2*, b) *E* and c) *Z1* after HPLC separation and silver complexation. To generate $[M+Ag]^+$ and $[2M+Ag]^+$ ions, 10 µM of $AgNO_3$ were added to the aqueous mobile phase.

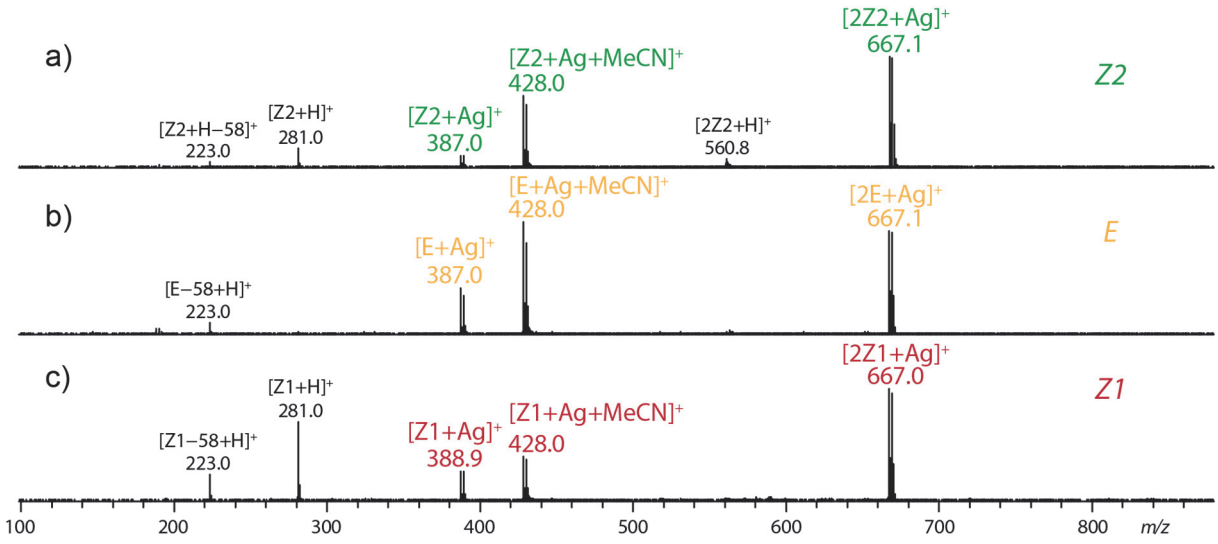

Figure S3. CID MS/MS spectra observed for a) $[Z2+Ag]^+$, b) $[E+Ag]^+$ and c) $[Z1+Ag]^+$.

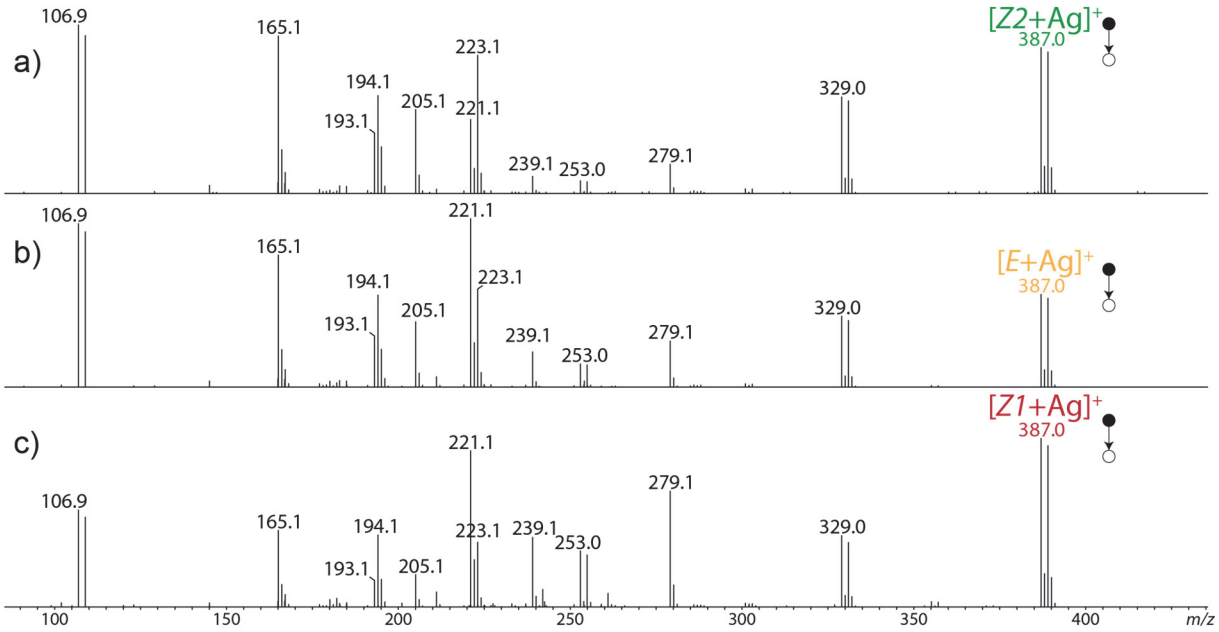

Figure S4. MS spectra observed for a) *Z2*, b) *E* and c) *Z1* after HPLC separation and calcium complexation. To generate $[3Z+Ca]^{2+}$ and $[4Z+Ca]^{2+}$ ions, 10 µM of $CaCl_2$ were added to the aqueous mobile phase.

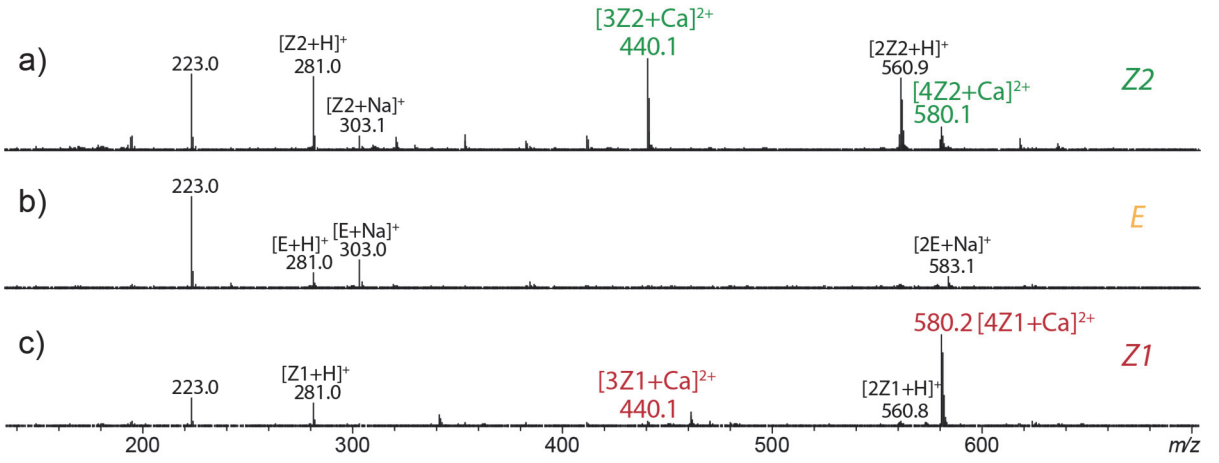

Figure S5. MS spectra observed for a) *Z2*, b) *E* and c) *Z1* after HPLC separation and zinc complexation. To generate Zn complex ions, 100 µM of $ZnSO_4$ were added to the aqueous mobile phase.

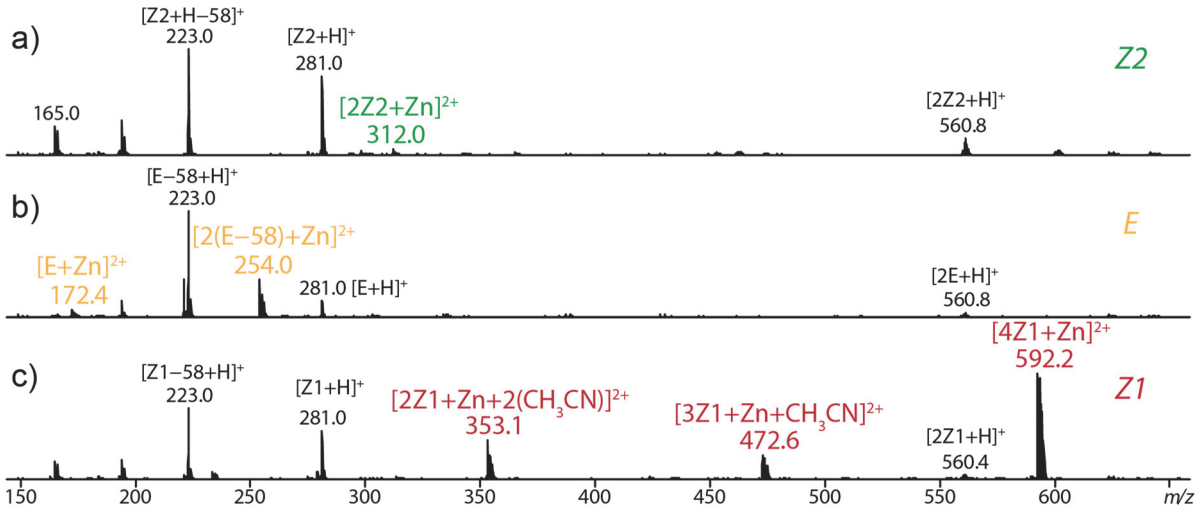

Figure S6. MS spectra observed for a) *Z2*, b) *E* and c) *Z1* after HPLC separation and iron complexation. To generate Fe complex ions, 100 µM of $FeCl_2$ were added to the aqueous mobile phase.

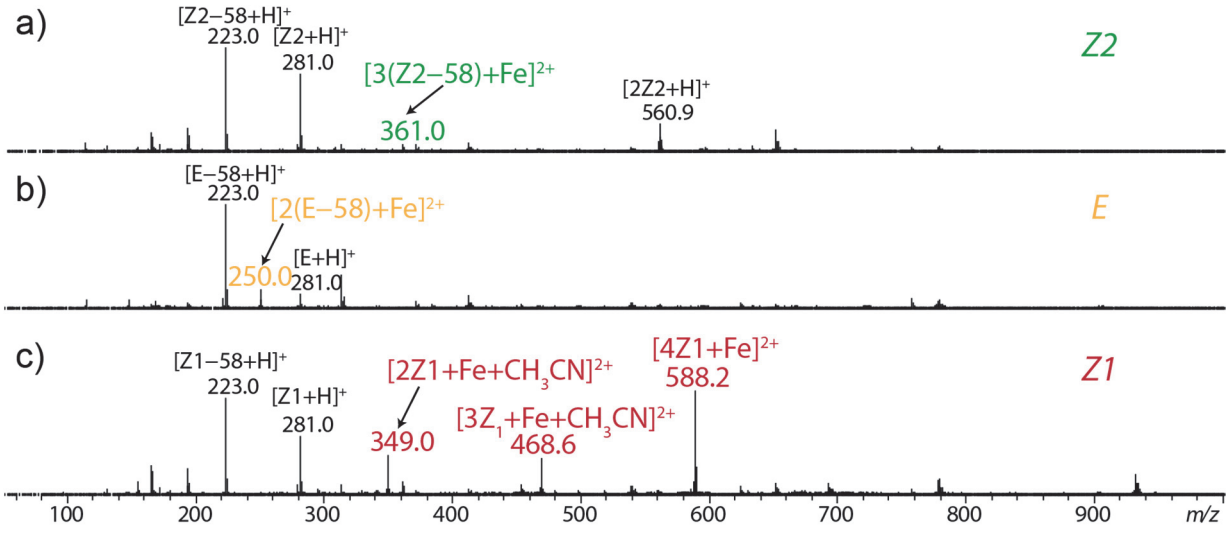

Figure S7. Relative HPLC peak integration area in function of the time used to determine the proportion of *E*→*Z1*/*Z2* isomers from LC-UV coupling for the different solvents at 30°C.

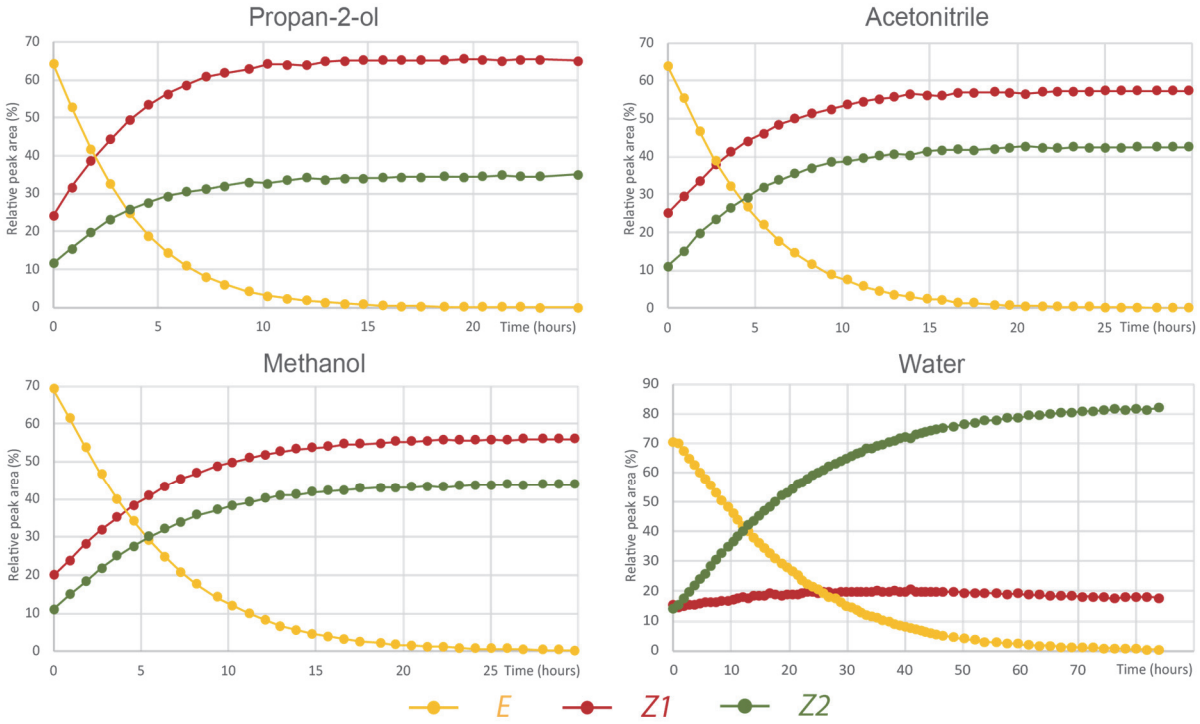

Figure S8. Relative HPLC peak integration area in function of the time used to determine the proportion of *E*→*Z1*/*Z2* isomers from LC-UV coupling for the different solvents at 40°C.

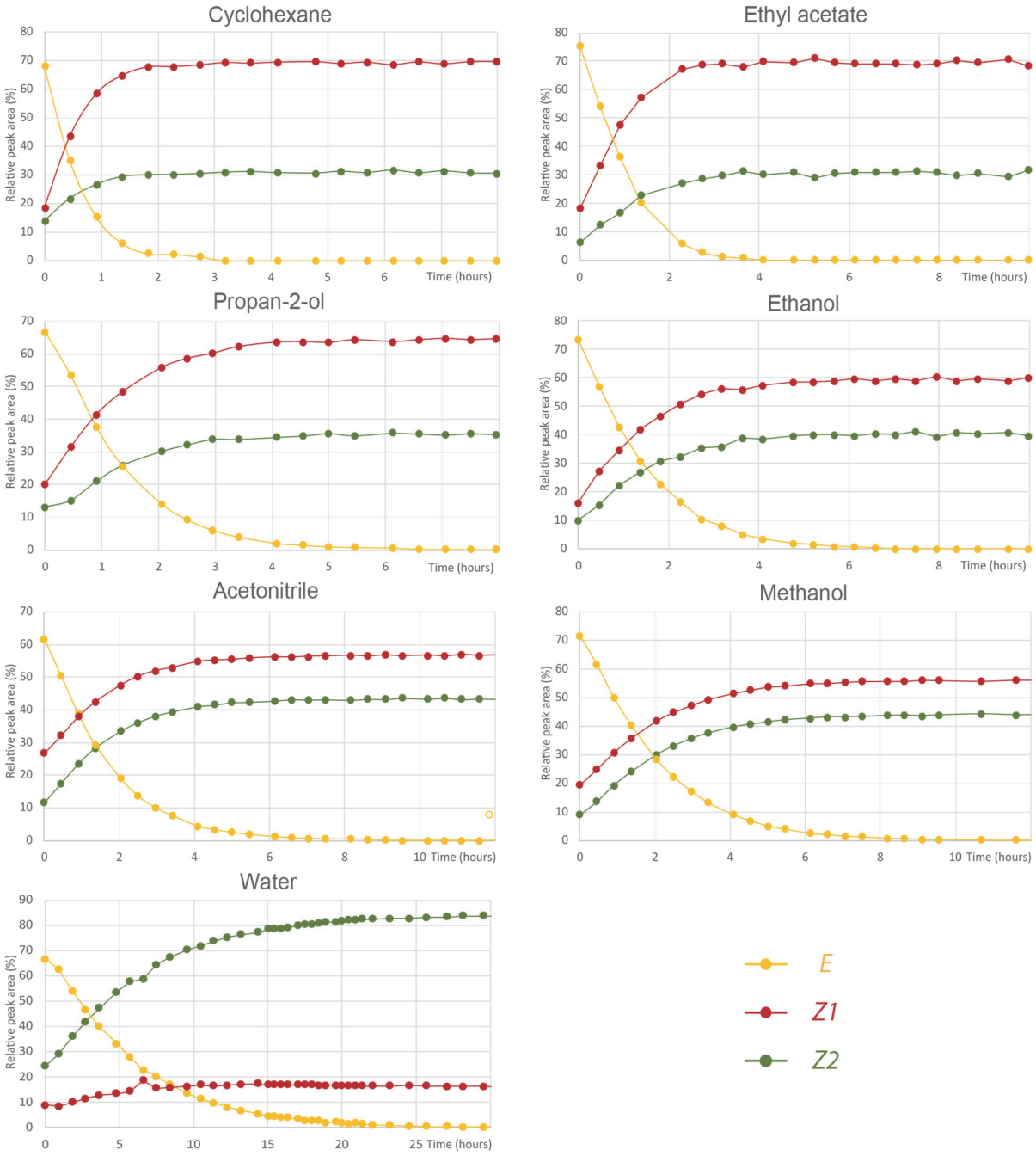

Figure S9. Plots ln[*E*] in function of the time from LC-UV experiments at 30°C.

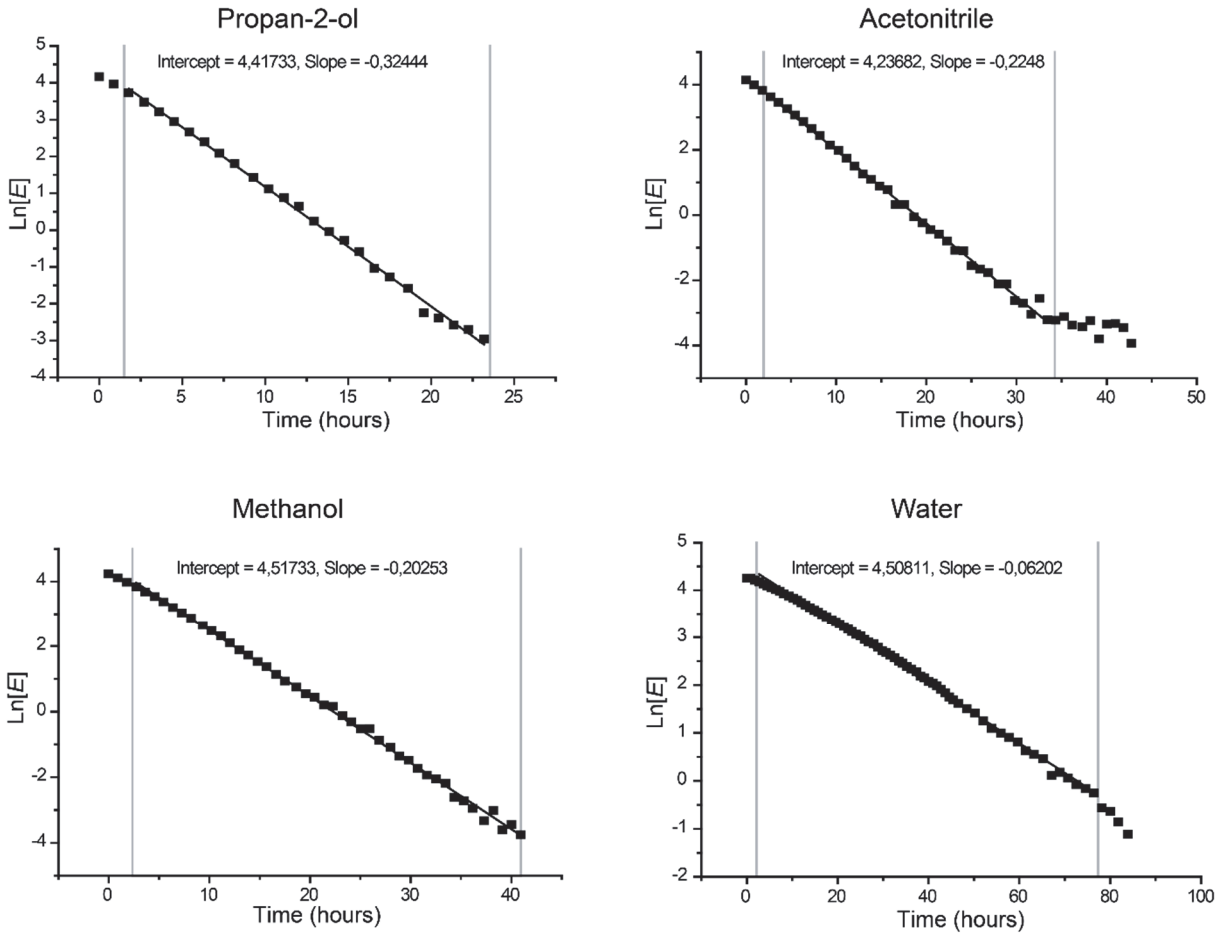

Figure S10. Plots ln[*E*] in function of the time from LC-UV experiments at 40°C.

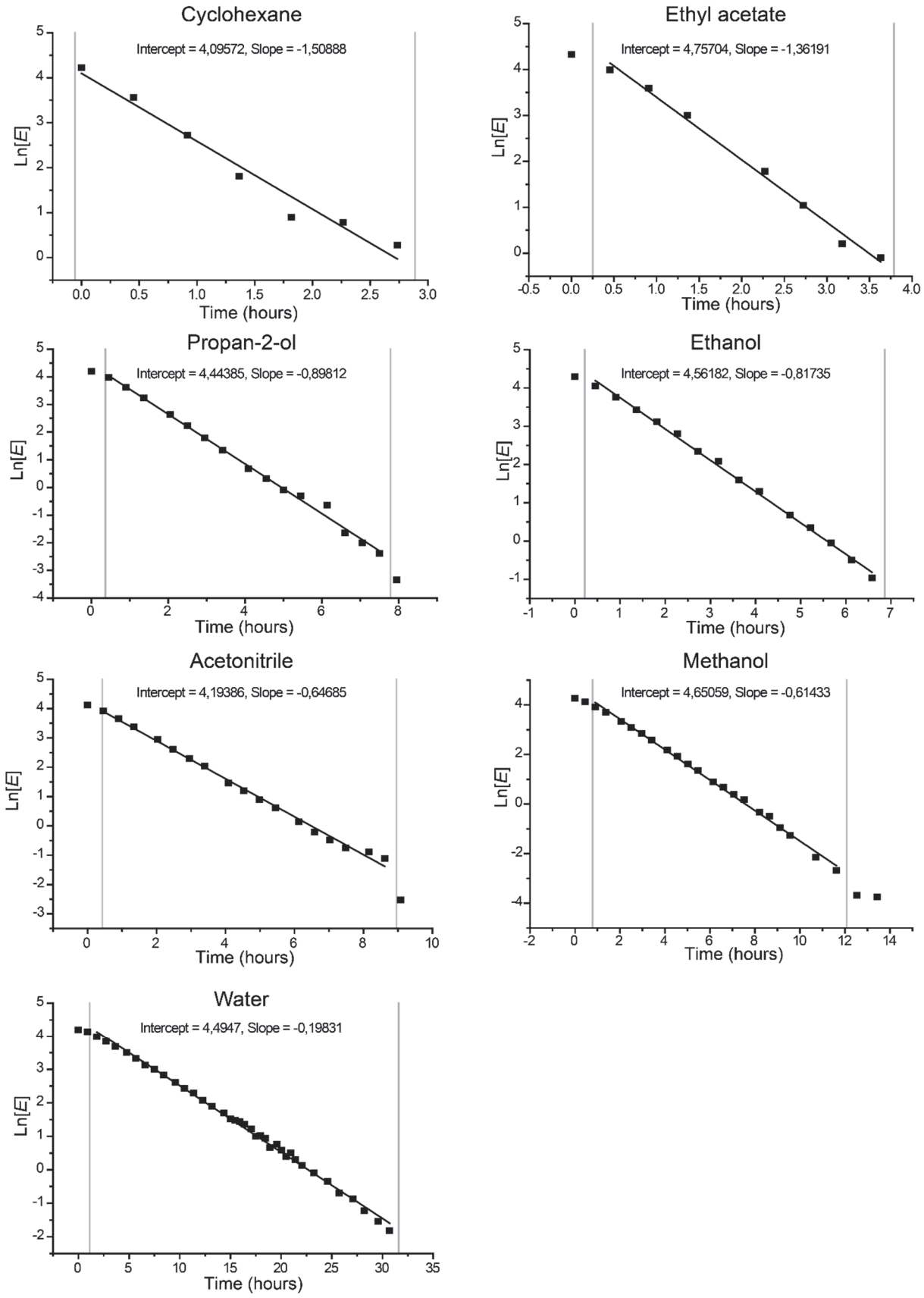

Figure S11. Extracted arrival time distributions of $[M+Ag]^+$ at *m/z* 387.0 obtained from drift tube ion mobility spectrometry after LC separation of a mixture of *Z1/Z2/E* isomers.

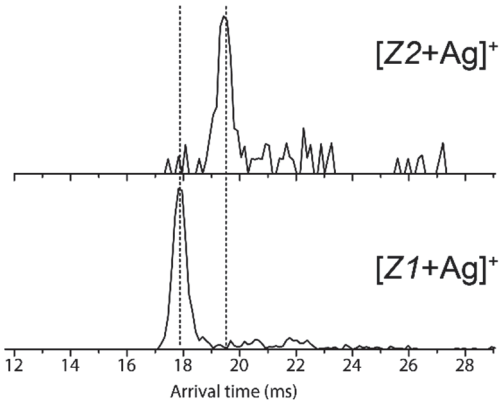

Figure S12. Extracted and fitted arrival time distributions of *m/z* 387.0 obtained from the first kinetic point of TWIMS-MS experiments at 50°C in different solvents.

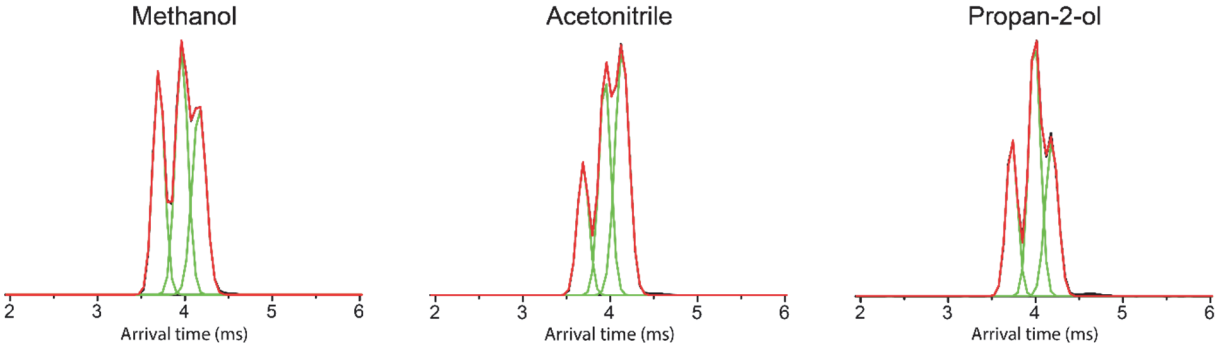

Figure S13. Structure of the various Ag^+ complexes optimized at the B3LYP/6-31G(d,p) level. Relative energies are given in kJ/mol.

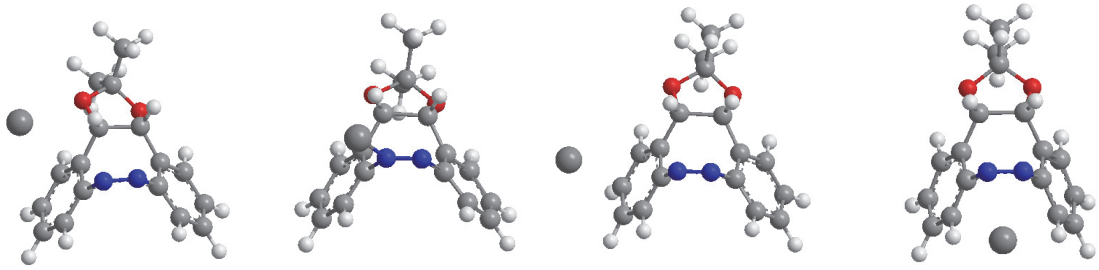

Z1_Ag1
+58.0

Z1_Ag2
26.6

Z1_Ag3
+65.4

Z1_Ag4
+20.2

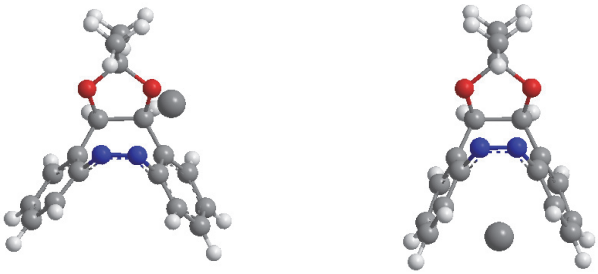

Z2_Ag1
0.0

Z2_Ag2
+37.7

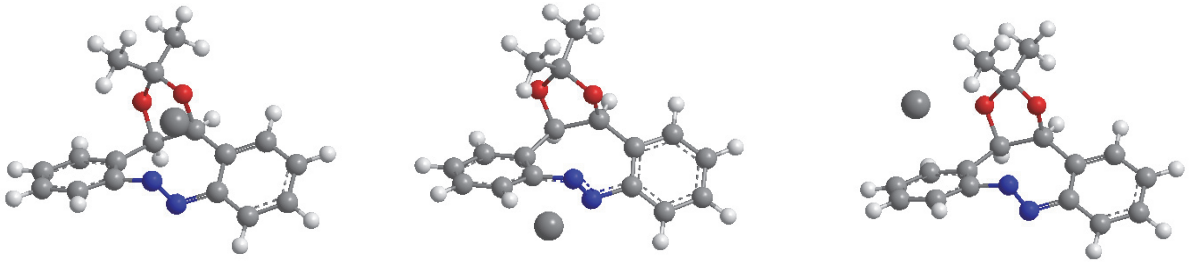

E_Ag1
+40.3

E_Ag2
+80.6

E_Ag3
+106.5

Table S2. Experimental and computed IR vibrational bands for the **Z1-Ag4** complex

Wavenumbers (cm^{-1})		DFT-computed intensities (km/mol)	Vibrational mode
Exp.	Calc.[a]		
780	763	102	γ CH benzenic
	786	30	γ CH benzenic
1042	1045	143	arom. ring breath.
1085	1089	107	ν C-O
1137	1149	20	δ C-H aro+ δ CH_3 wag.
1180	1195	198	δ CH_2 sciss. of CH_3
	1218	34	δ CH aliph.
1227	1241	58	δ CH aliph.
1349	1374	33	δ CH_3 umbrella
1398	1413	21	δ CH arom.

a) Scaled by a factor of 0.965

Table S3. Experimental and computed IR vibrational bands for the **Z2-Ag1** complex

Wavenumbers (cm^{-1})		DFT-computed intensities (km/mol)	Vibrational mode
Exp.	Calc.[a]		
748	746	61	γ CH benzenic
	755	32	γ CH benzenic
975	957	55	γ CH CH_3
1025	1019	118	ν C-O
1142	1137	57	δ CH_2 rock.
1200	1190	106	δ CH CH_3
	1203	75	δ CH arom.
1235	1244	40	δ CH CH_3
1365	1364	34	δ CH_3 umbrella

a) Scaled by a factor of 0.965

Figure S14. DFT calculated IR absorption spectrum for the optimized structures of the [*Z1*+Ag]$^{+}$ complex

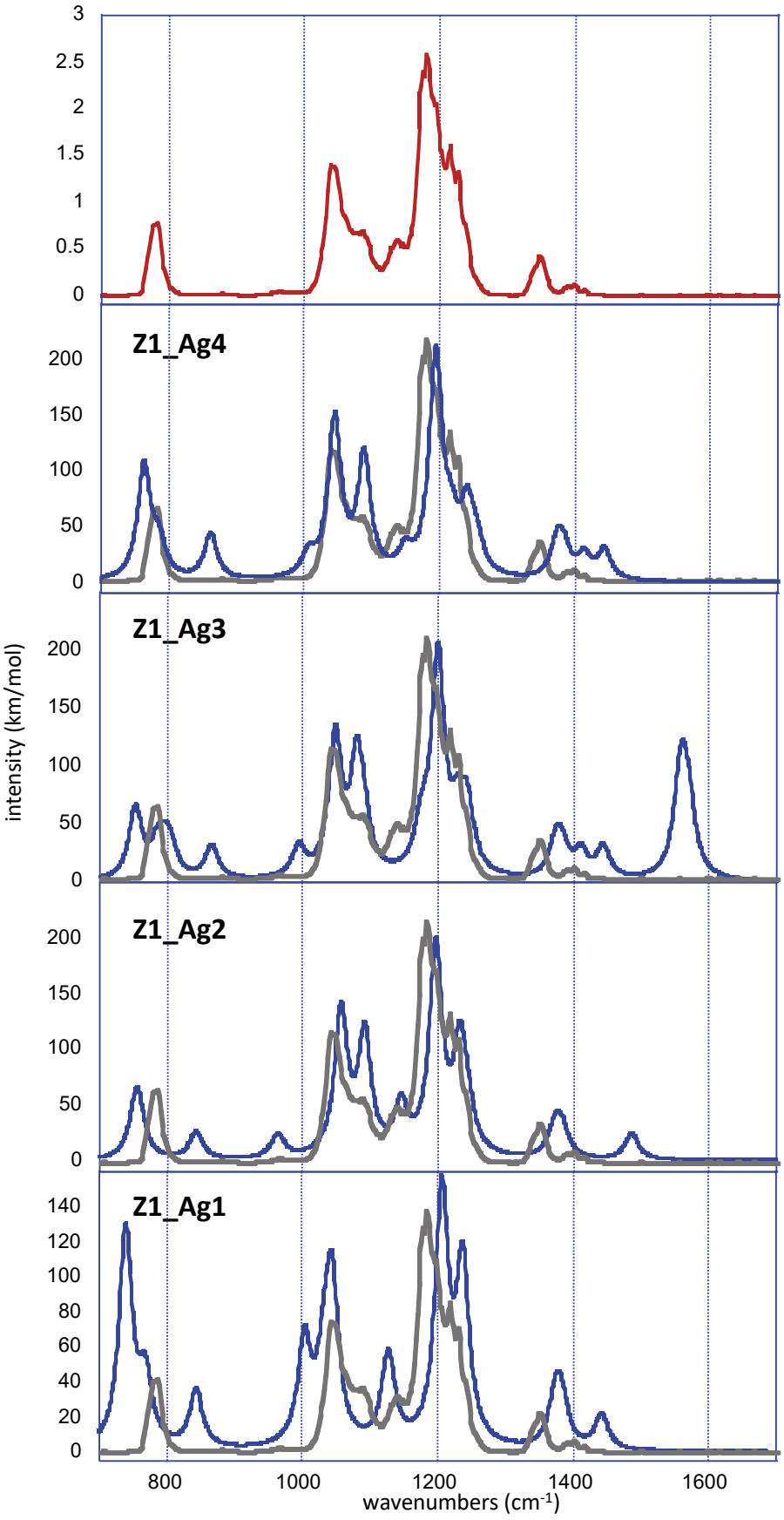

Figure S15. DFT calculated IR absorption spectrum for the optimized structures of the [*Z1*+Ag]$^+$ complex

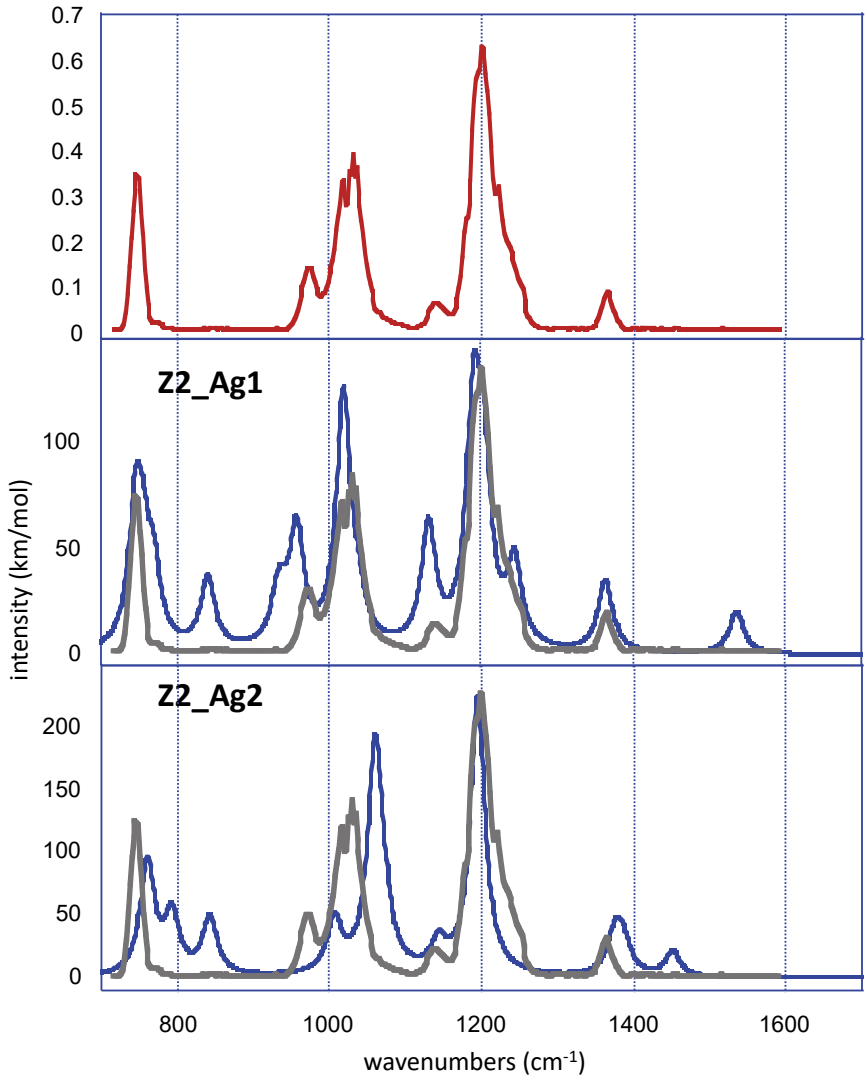

Table S4. Experimental CCS values obtained from drift tube ion mobility experiments and theoretical CCS values obtained with the TM, PA and EHSS algorithms of the MOBCAL software.

	Experimental	Theoretical		
		TM	PA	EHSS
Z1 (Z1_Ag1)	106 ± 2 Å²	101 Å²	106.9 Å²	115 Å²
Z1 (Z1_Ag2)		101.9 Å²	112.4 Å²	121.3 Å²
Z1 (Z1_Ag3)		102.5 Å²	110.4 Å²	119.4 Å²
Z1 (**Z1_Ag4**)		**96.3 Å²**	**101 Å²**	**107.2 Å²**
Z2 (**Z2_Ag1**)	115 ± 2 Å²	**97.1 Å²**	**106,4 Å²**	**114.1 Å²**
Z2 (Z2_Ag2)		115.0 Å²	93.5 Å²	100.4 Å²

Figure S16. Plots of intensities ratio of $[E+Ag]^+/[2E+Ag]^+$ in function of the time from IMS-MS experiments at 60°C.

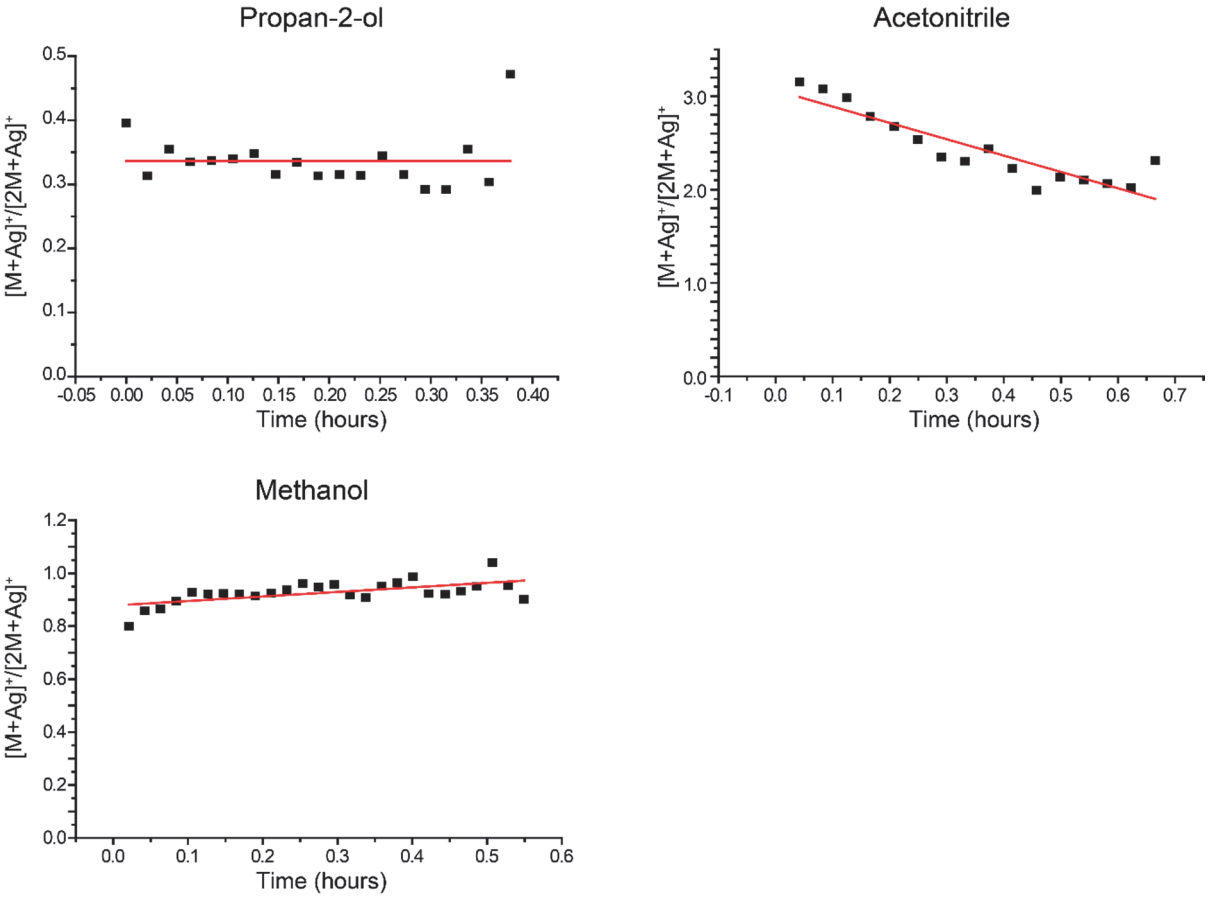

Figure S17. Plots ln[*E*] in function of the time from IMS-MS experiments at 50°C.

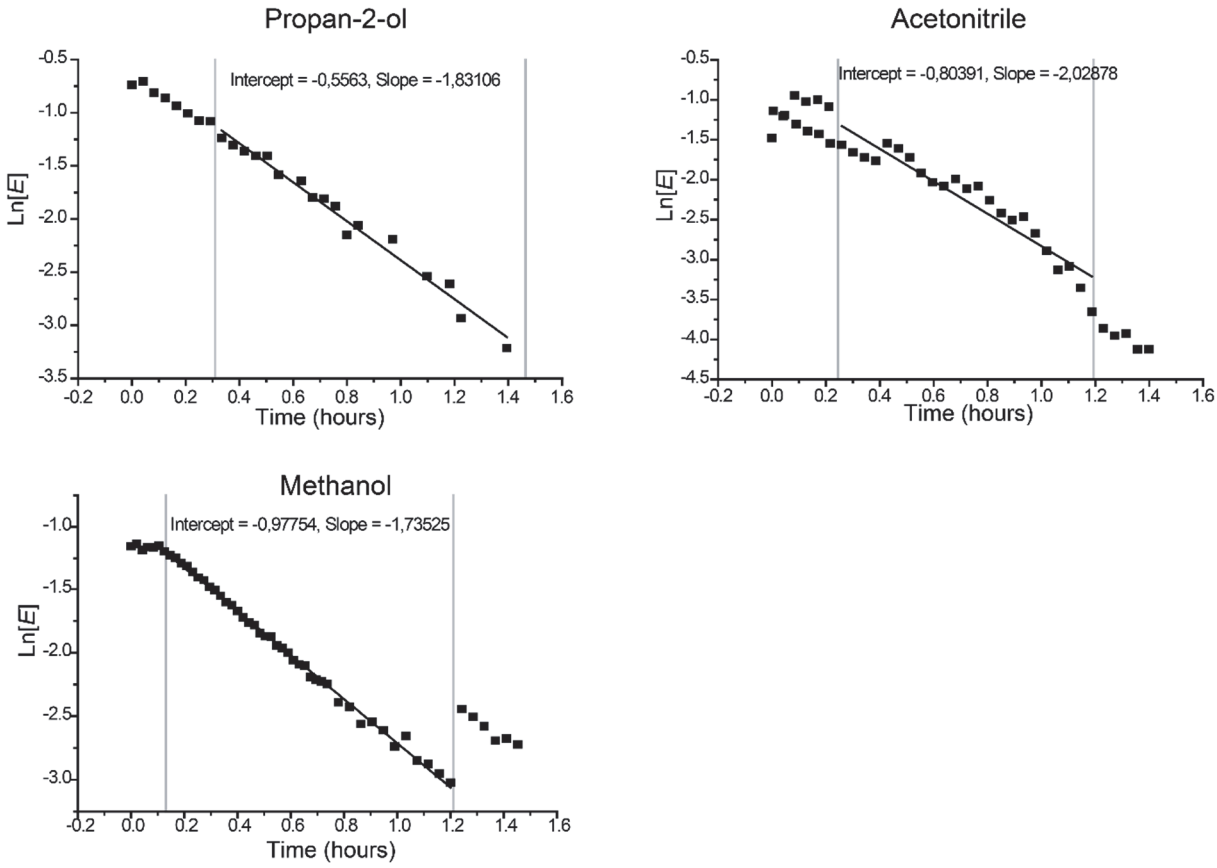

Figure S18. Plots ln[*E*] in function of the time from IMS-MS experiments at 60°C.

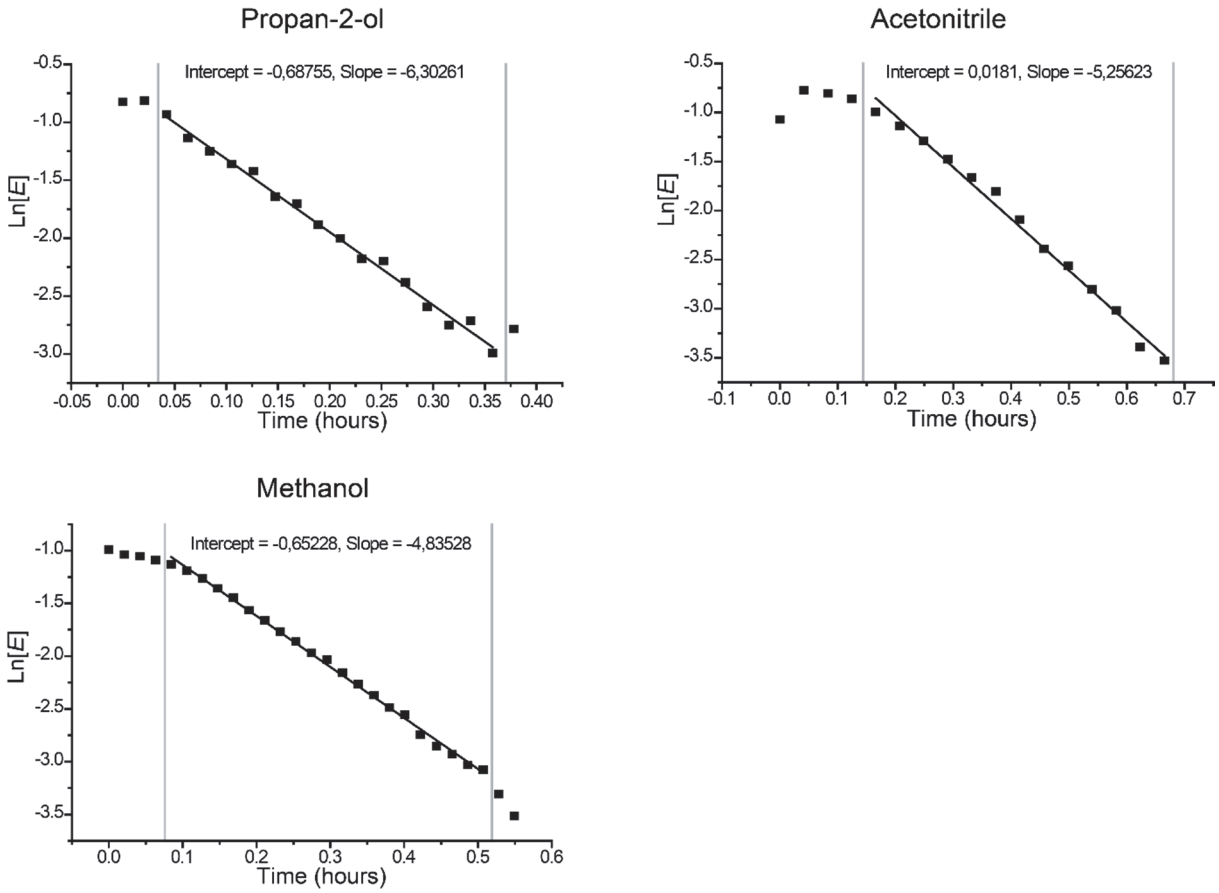

Figure S19. Plots ln[*E*] in function of the time from IMS-MS experiments at 70°C.

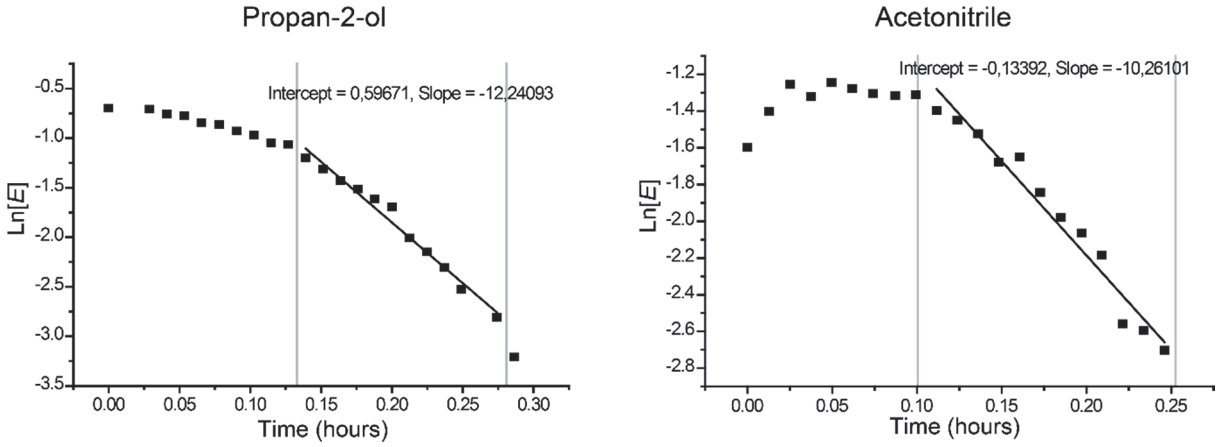

Figure S20. Plots ln[*E*] in function of the time from a) LC-UV and b) IMS-MS experiments at 40°C.

a) LC-UV experiments

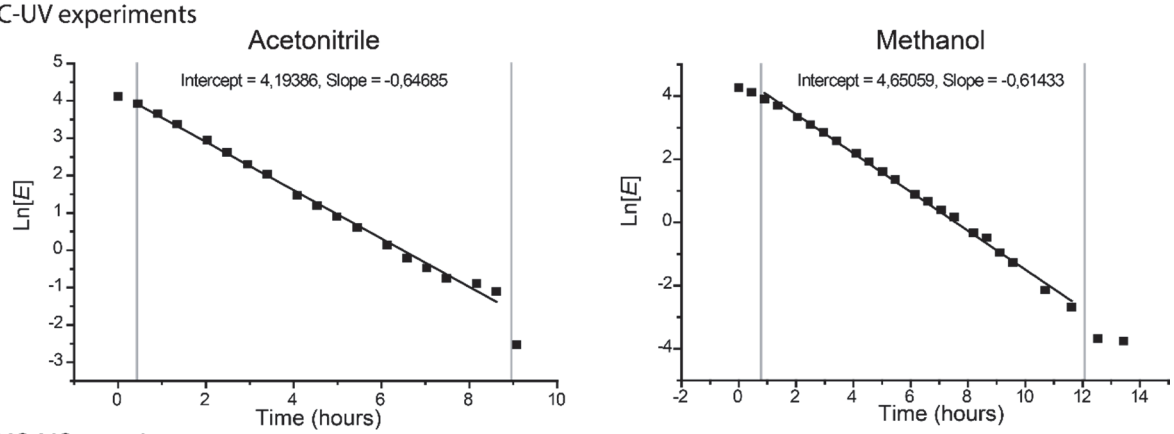

b) IMS-MS experiments